AD-A122 569 THE STRUCTURE AND ENERGY BUDGET OF THE HEAT LOW OVER THE EMPTY QUARTER IN..(U) NAVAL OCEAN RESEARCH AND DEVELOPMENT ACTIVITY NSTL STATION MS.. 1/1

UNCLASSIFIED D W BLAKE ET AL. SEP 82 NORDA-TN-170 F/G 20/13 NL

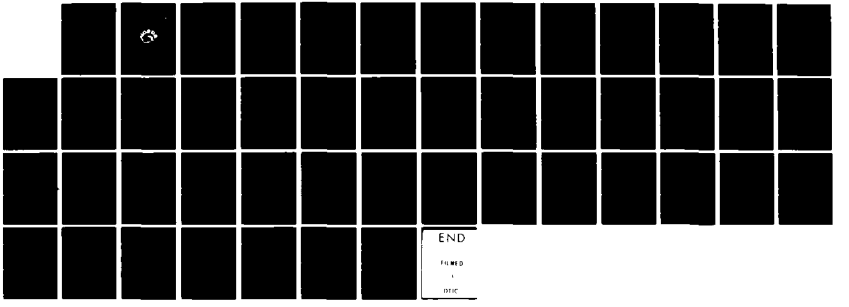

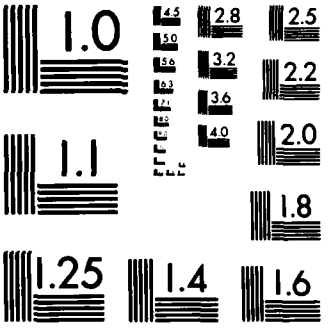

MICROCOPY RESOLUTION TEST CHART
NATIONAL BUREAU OF STANDARDS-1963-A

(12)

NORDA Technical Note 170

Naval Ocean Research and
Development Activity
NSTL Station, Mississippi 39529

The Structure and Energy Budget of the Heat Low Over the Empty Quarter in Saudi Arabia During May 1979

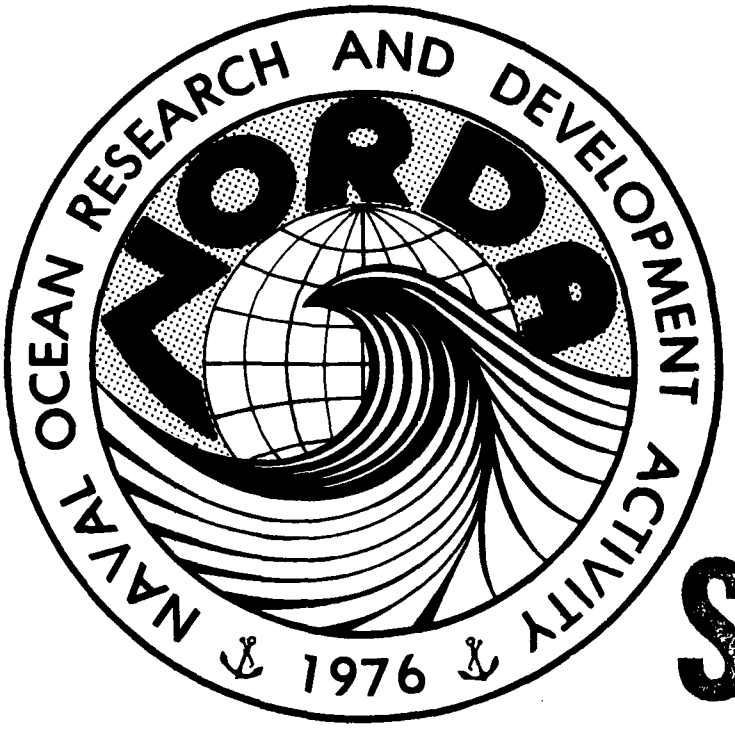

D.W. Blake
Numerical Modeling Division
Ocean Science and Technology Laboratory

J.S. Fein
National Science Foundation
Washington, D.C. 20550

T.N. Krishnamurti
S.V. Low-Nam
Department of Meteorology
Florida State University
Tallahassee, Florida 32306

September 1982

ABSTRACT

In this paper we present an analysis of a unique data set over the desert area of Saudi Arabia during the northern summer months. The data set comes from the GARP Monsoon Experiment. The analysis reveals a unique vertical structure of the atmosphere above the heat low. The analysis of the thermodynamic data reveals that a well-mixed layer extends to 650 mb during the day and a stable configuration exists during the night. Calculations of divergence and vertical motions show that over this region the entire troposphere is dynamically active with strong descending motions above a surface layer about 1 km deep within which rising motions are found during the day. Descending motions extend to the surface at night. A description of the vertical distribution of the short and longwave radiative processes over this region, based on detailed aircraft observations, is included. The new results here are the large magnitudes of heating by solar radiation ($\approx 6^{o}C$/day) and a comparable cooling by the longwave radiation. The net radiation profile in the day exhibits a net warming in the middle troposphere and a net cooling near the surface layer. This contributes to stabilization of the mixed layer.

The paper addresses the thermodynamic budget over the heat low. We examine the role of the horizontal and vertical advective processes, radiative processes, and the vertical eddy flux convergence in the maintenance of the tropical stratification.

Satellite observations show that the desert area experiences a net loss of radiation to outer space, while the thermal stratification remains nearly invariant from one day to the next. This study shows that a crucial element in the maintenance of the stratification is the import of heat into this region in the tropical upper troposphere. This energy supply most likely comes from planetary scale divergent circulations.

ACKNOWLEDGEMENTS

This work was funded jointly by ONR program element 61153N, "Numerical Studies in Ocean Dynamics," under Program Manager Dr. Herbert Eppert and by a grant from the National Science Foundation to Florida State University, NSF Grant No: NSF ATM-78-19363. The computations described here were carried out at the computer facilities at the Naval Research Laboratory; at Florida State University; and at the National Center for Atmospheric Research, which is sponsored by the National Science Foundation.

1. Introduction

The thermodynamic budget of the heat lows over the desert region of North Africa and Arabia is an important problem. Charney (1975) emphasized the anomalous nature of the earth's radiation budget over these regions. He noted that, while in general the net incoming minus the outgoing radiation is positive over the tropics and negative over the higher latitudes, a major exception is the desert regions. Here the satellite measurements show that the net outgoing radiation exceeds the incoming radiation. The vertical stratification of temperature and humidity remains nearly invariant from one day to the next (except for the diurnal component). Under these circumstances the mechanisms for the maintenance of the stratification, in the presence of large energy losses at the top of the atmosphere, is an interesting problem. The energy balance must require lateral import of energy from the surrounding regions since there are no known non-radiative sources within these dry desert regions. Moist convective heating is not an important energy source; the dry convective heating is related to the warm soil temperature which is determined by the radiative heat balance of the earth's surface.

This study addresses the following issues related to the maintenance of the thermal stratification of the heat low:

a) The design of a field experiment for determining the mass and thermodynamic budgets.

b) Analysis of data sets to determine the observed structure of the heat low.

c) Determination of the depth of the mixed layer.

d) The vertical structure of the divergence and vertical motion field. This part provides information on the vertical levels where mass flux is directed into or out of the general regions of the heat low.

e) The thermodynamic heat balance of this region provides information on the vertical levels where energy is imported to maintain the thermal stratification.

The study also addresses the differences in the analysis of results for daytime observations versus those made around the early morning hours.

3. The Field Experiment

The field experiment was conducted during the summer MONEX Phase (a list of acronyms appears in Table 1) of the Global Experiment in 1979. The experiment largely consisted in the enhancement of the usual World Weather Watch data sets with those obtained from a sophisticated research aircraft, the NASA CV990. In addition, the data sets from TIROS N, a polar orbiting satellite, provided measurements for some components of the earth's radiation budget.

The NASA CV990 flew three missions over the Empty Quarter of Saudi Arabia following the general flight plan shown in Fig. 1: two during the day (9 and 10 May 1979) and one during the night (12 May 1979). The pattern was chosen to cover the largest possible area subject to restrictions of fuel range and flight considerations. In Fig. 1 the arrows show the flight direction and the numbers

indicate the order in which the dropsondes were deployed. Note that dropsonde #2 and dropsonde #10 were launched in the same location but were separated in time by approximately four hours. This spacing permitted a check on the time variation of the measured parameters. In general, the launches of the dropsondes were spaced to avoid signal interference. After dropsonde #3 was launched the plane descended in a stair-stepping pattern from the cruising altitude of about 250 mb (11,000 m) down to about 930 mb (750 m above the surface of the desert) before climbing back to the cruising altitude for the launch of dropsonde #4. During the stair-stepping pattern onboard measurements were made at the various altitudes of the upward and downward irradiances of longwave and shortwave radiation. Detailed information on the onboard radiation instrumentation and the radiation data sets is given by Ackerman and Cox (1982).

The 00Z sea level pressure distributions for 9, 10 and 12 May 1979 are illustrated in Figs. 2a-c, respectively. The surface heat low is centered to the south of the flight path on the 9th and 10th of May and to the southeast on the 12th of May. Additional surface data for the Empty Quarter is scarce as the only nearby surface station is Sheroara which is about 150 km south of the flight path (Fig. 1). The surface pressure and temperature as a function of time is shown in Fig. 3 for 10 May 1979. The temperature exhibits a strong diurnal variation: (1) minimum of 26°C from 0300 and 0900 LST, (2) an abrupt increase after sunrise between 0800 and 0900 LST, (3) a nearly uniform temperature maximum of 38°C from 1100 to 1700 LST, and (4) a slow decrease from 1700 LST (just before sunset) to 0300 LST. The pressure shows a strong semidiurnal variation: (1) a maximum of 1013 mb between 0800 and 1100 LST, (2) a minimum of 1008 mb at 1600-1700 LST, (3) a secondary minimum of about 1009 mb between 2300 and 0100 LST. The pressure and temperature variations are similar for the 9th and 12th of May. Flight times for the two daytime missions (9 and 10 May) were centered about the time of the surface temperature maximum. For each daytime mission, a comparison of data from dropsondes #2 and #10 (Fig. 1), separated in time by 3.5 to 4 hours, shows little temporal variation. Therefore, all data from a given daytime flight are treated as being synoptic in the present context. On the other hand, an early morning flight (12 May) originated at 0400 LST, and ended around 1000 LST. Discernible differences in all dropsonde data taken before and after sunrise were noted. Comparison of data from dropwindsondes #2 and #10 (launched before and after sunrise, respectively) show considerable differences. For this reason only the pre-sunrise data (prior to 0700 LST) are treated as nighttime data, and the remaining observations for these data are not considered in this study. The parameters measured by the dropwindsondes are horizontal winds, temperature, pressure and relative humidity. The onboard instruments provided winds, temperature, relative humidity, altitude, pressure, and the upward as well as the downward long and shortwave irradiances. No differentiation is made between onboard and dropsonde data. (For a more complete summary of the objectives and experiments of Summer MONEX, see the Summer MONEX Field Phase Report, 1981.)

3. Analysis of the Data Sets

The analysis of the data for temperature, horizontal winds, and relative humidity proceeds as follows: The location of each point is given in terms of latitude and longitude which are converted into an orthogonal x, y coordinate system with its origin at 15°N, 42°E. The area considered is the trapezoid extending from 42°E to 60°E and from 15°N to 30°N. The atmosphere between 1000 mb

and 200 mb is divided into eight layers, each 100 mb thick and each datum point is assigned to the appropriate layer. The number of data points in each layer for each mission is indicated in Table 2; all data points in a layer are treated as occurring at the midlevel for that layer. Standard multiple linear regression techniques are used to analyze the data as a function of the east-west coordinate, x, and the north-south coordinate, y. For example, the east-west wind is expressed via a linear regression:

$$u_i = a_i x + b_i y + c_i \qquad i = 1, 2, \ldots, 8 \qquad (1)$$

where the subscript refers to the layer (1 is the layer centered at 950 mb). The mean value for each parameter is determined by averaging over the area described above; the east-west wind in Eq. 1 may be expressed by:

$$u_i = [u]_i + u_i^* \qquad (2)$$

where brackets denote the area-averaged value and the asterisk denotes the deviation of the east-west wind from its area-averaged value over the area. In Table 2 the smallest number of data points per layer occurs for the mission of 12 May 1979 since we limited the data to the pre-sunrise hours. For this mission finer vertical resolution would result in too few data points per layer for the satisfactory application of the multiple linear regression techniques. Furthermore, the analysis is restricted to linear regression as both the number of data points per layer and the small domain size do not justify considering quadratic or higher order regression.

4. The Thermal Structure and the Depth of the Mixed Layer

In this section we shall describe the vertical structure of the thermal field over the Saudi Arabian desert. For this purpose we require a representative measure of the horizontal area-averaged potential temperature. This is accomplished by an analysis of the potential temperature via the linear regression and a subsequent averaging over the domain (42°E, 60°E, 15°N, 30°N). The resulting mean potential temperatures for the three missions are illustrated in Fig. 4 together with the potential temperature profile of the U. S. Standard Atmosphere at 15°N. For completeness, the surface values are plotted from the Sheroara station for each sounding. The potential temperature profiles for the 9 May and 10 May missions, are for the same time of day, differ less than 2 K at all levels and by less than 1 K at most levels. However, compared to the potential temperatures for either daytime mission, those for the 12 May missions are cooler above 300 mb and below 900 mb and up to 2.5° K warmer at levels in between. Above 750 mb and below 300 mb, the potential temperature at a given level for the U. S. Standard Atmosphere generally lies within the range of potential temperatures found for the three missions. We also noted that between 500 and 550 mb, the potential temperatures for all four profiles were within 1/2 K of each other. This implies that the diurnal change is quite small in the middle troposphere. The largest variations in potential temperature occur in the lowest levels and at the surface. The minimum nighttime temperature at the Sheroara station is 10-15 K cooler than the maximum daytime temperature, reflecting the expected diurnal variation (see Fig. 3). The ground surface or the soil temperature, as measured by onboard instruments, shows even larger diurnal fluctuations of about 25 K. On the 12 May

mission we watched the onboard printout of the ground temperature as the sun rose. Within 45 minutes it changed from the pre-sunrise value of 24°C to 48°C, an increase of 1/2°C per minute. Aside from the diurnal variations, below 750 mb the atmosphere above the Empty Quarter is considerably warmer up to 12 K at 950 mb -- than the U. S. Standard Atmosphere as would be expected for the atmosphere above a large, hot desert.

During the day and above the surface layer at night, the potential temperature is approximately constant up to 650 mb, indicating a well-mixed layer up to this level. The specific humidity (Fig. 5), although varying on different days, also indicated a well-mixed layer up to 650 mb.

5. Vertical Structure of Divergence and Vertical Velocity

The magnitude and direction of the horizontal wind for the May 9 mission for various locations and altitudes are displayed in Figs. 6a-h. Similar displays for the 10 May and 12 May missions are shown in Figs. 7a-h and 8a-h, respectively. Several features of the analysis are of interest. The cyclone at the surface (Fig. 2a), which is associated with the intense heating became anticyclonic above 800 mb. Above 600 mb we note passage of waves in the westerlies with the winds as large as 40 m/sec in the upper troposphere. Kinematic vertical velocity is derived from integrating the continuity equation

$$\omega(p) = \omega(p_0) - \int_{p_0}^{p} (\vec{\nabla} \cdot \vec{v})\, dp \qquad (3)$$

where p_0 is the surface pressure. The horizontal divergence is calculated after the eastward wind component, u, and the northward wind component, v, have been analyzed as in Section 3. Thus,

$$u_i = a_i x + b_i y + c_i$$

and

$$v_i = d_i x + e_i y + f_i \qquad i = 1, 2, \ldots, 8 \qquad (4)$$

yield the horizontal divergence:

$$\vec{\nabla} \cdot \vec{v} = a_i + e_i \qquad i = 1, 2, \ldots, 8 \qquad (5)$$

The general assumption that $\omega(p_0) = 0$ and $\omega(0) = 0$ requires two boundary conditions which cannot be satisfied simultaneously because the divergence, calculated from the observations, contains experimental errors. To handle this difficulty, a correction to the divergence is applied, which is given by the relation,

$$\vec{\nabla} \cdot \vec{v})_c = \vec{\nabla} \cdot \vec{v})_u + \varepsilon\, |\vec{\nabla} \cdot \vec{v}|_u \qquad (6)$$

Here we assume that the error in divergence is proportional to the magnitude of divergence. This is a standard procedure for correcting the divergence; the coefficient ε is given by

$$\varepsilon = \frac{\int (\vec{\nabla} \cdot \vec{v})_u \, dp}{\int |\vec{\nabla} \cdot \vec{v}|_u \, dp} \tag{7}$$

The limits of the integral are from bottom to top of the atmosphere; ε is a constant. However, this simple approach for the determination of ε was abandoned after carrying out a preliminary analysis of the heat balance. As noted earlier, we found that the time tendency of potential temperature was extremely small at 500 mb. Furthermore this level lies above the mixed layer; hence we expect at this level large scale thermodynamic balance between the horizontal and vertical advective terms and the radiative forcing. This observation was used as a test of the aforementioned divergence correction. We noted that the choice of single constant value for ε did not provide a reasonable balance at 500 mb. In order to overcome this difficulty, a two parameter approach was followed. Here we let ε vary linearly with pressure, i.e.,

$$\varepsilon_i = \alpha p_i + \beta, \qquad i = 1, 2, \ldots, 8 \tag{8}$$

Two constraints are required to determine the constants α and β. One of these, of course, is a requirement that the vertically integrated divergence vanish, the other constraint is to require that thermodynamic balance at 500 mb be satisfied by the large scale advective and radiative processes. The adjusted vertical motions satisfy the two boundary conditions,

$$\omega = 0, \qquad p = 200, 1000 \text{ mb} \tag{9}$$

The choice of p = 200 mb as an upper boundary was made because no detailed observations of divergence were available above the maximum altitude of the aircraft flights which was around 250 mb. The corrected horizontal divergences and vertical motions for 9 May and 10 May are illustrated in Figs. 9a and 9b, respectively. The profiles for these two daytime missions are quite similar and indicate that there are two circulation cells in the vertical:

(1) the lower, shallow cell has surface convergence in the heat low, rising air and divergence at 850 mb, and

(2) the upper, deeper cell, starting with divergence at 850 mb, has descending air with weak convergence above this level.

On the other hand, the corrected horizontal divergence and vertical motions for the nighttime calculations (Fig. 9c) indicate the presence of one cell with sinking air at all levels; convergence is noted above 550 mb and divergence is found below 550 mb. The reversal in sign of the low level divergence to low level convergence between night and day is consistent with the pronounced heating during the day. The soil as well as the air temperature exhibits a pronounced diurnal cycle as does the net radiation. The large change in dry static stability between night and day also seem consistent with the profiles of divergence. A more detailed examination of this follows in the next section.

6. Heat Budget

The first law of thermodynamics is expressed by the usual relation

$$\frac{d\theta}{dt} = \left(\frac{1}{c_p}\right)\left(\frac{p_0}{p}\right)^{R/c_p} \sum_j H_j \tag{10}$$

(a list of symbols appears in Table 3); here H_j denotes the net energy added per unit mass per unit time due to various sources, j. The energy sources include longwave (j = L) and shortwave (j = S) irradiances; the latent heat release is neglected over this region. With the aid of the continuity equation, the resultant thermodynamic equation is averaged over the domain and an equation for the energy budget is written as:

$$\underset{(1)}{\frac{\partial[\theta]}{\partial t}} = \underset{(2)}{-[\vec{v}]\cdot[\vec{\nabla}\theta^*]} \underset{(3)}{-[\omega]\frac{\partial[\theta]}{\partial p}} + \underset{(4)}{\frac{1}{c_p}\left(\frac{p_0}{p}\right)^{R/c_p}[\sum_j H_j]} \underset{(5)}{-[\vec{\nabla}\cdot\vec{v}^*\theta^*]} \underset{(6)}{-\frac{\partial}{\partial p}[\omega^*\theta^*]} \tag{11}$$

where $\vec{\nabla} = \hat{i}\,\partial/\partial x + \hat{j}\,\partial/\partial y$, the brackets denote the average or mean over the domain, and the asterisks denote the deviations from the mean values. Term (2) denotes the mean horizontal advection of heat, and term (3) denotes the mean adiabatic heating. These two terms can be calculated directly from the results found in Sections 4 and 5. Term (4) the net radiative heating, is calculated from the measurements made by the Colorado State University team (Smith, Ackerman, Cox, and Vonder Haar, 1980). As was discussed in Section 2, the flight time for each mission was chosen in an attempt to minimize the local time rate of change of mean potential temperature, i.e., term (1). The mean horizontal convergence of eddy heat flux, term (5), generally is considered to be small compared to the other terms and will be neglected here. Finally, term (6), the sensible heat flux of the vertical variation of the mean convective and turbulence heat flux, is calculated as a residual in Eq. (11), once the other terms are known. Convection is triggered in regions of the atmosphere which are statically unstable, over regions with superadiabatic lapse rates. The ground temperature, measured between longitudes 52°E and 50°E, during aircraft flights at about 750 m above the desert surface, was around 46°C (319 K) for 9 May and around 50°C (324 K) for 10 May. As the ground is much hotter than the air above it, a strong temperature drop in the lowest few meters above the surface was present. Over this region of the superadiabatic lapse rate, parcels rise until they reach an equilibrium level with the same potential temperature which can be as high as 600 mb if mixing is ignored.

The flux measurements for the upward and downward components of both longwave and shortwave radiation for the 9 May mission are presented in Figs. 10a-d.

Similar displays for the 10 May and 12 May missions are shown in Figs. 11a-d and 12a-d, respectively. The measurements shown here were taken directly from the onboard computer printout of experimental results, and have not been corrected for changes in the plane's pitch and roll (Smith et al., 1980). In particular, the instruments were pointed off the vertical axis as the research aircraft descended from one level to the next in the stairstepping pattern. At each level the plane flew horizontally for several minutes permitting the instruments, now pointed directly up and down along the vertical axis, to stabilize. In order to compensate for these effects, a smooth curve has been fitted to the "stabilized" measurements for each of the four components of flux, as illustrated in Figs. 10a-d, 11a-d, and 12a-d. The net radiative heating rate, term (4) in Eq. (11), is the sum of the net longwave radiative heating, T_L, and the net shortwave heating rates, T_S. These two quantities, T_L and T_S, were calculated using

$$T_j = \frac{1}{c_p} \left(\frac{p_0}{p}\right)^{R/c_p} H_j \qquad j = L, S \tag{12}$$

and

$$H_j = g \left(\frac{\partial F_{jU}}{\partial p} - \frac{\partial F_{jD}}{\partial p}\right) \qquad j = L, S \tag{13}$$

where F = flux (radiant flux density), and the subscripts U and D refer to upward and downward, respectively. The flux values used in Eq. (13) are taken from the fitted curves in Figs. 10a-d, 11a-d, and 12a-d.

Figs. 10a-d and 11a-d illustrate the vertical distribution of the up and down radiative fluxes during the daytime. About 1150 watts/m^2 of solar energy is received at the 250 mb level; this amount is depleted to about 900 watts/m^2 by the 950 mb level. Thus, about 250 watts/m^2 of the incident energy is absorbed by the troposphere. About 375 watts/m^2 of the incident solar radiation is reflected at the earth's surface (implying a surface albedo of around 40%). The upward directed shortwave irradiance is nearly a constant over most of the troposphere. Downward irradiance of longwave radiation increases in the troposphere from about 100 watts/m^2 (at the 300 mb surface) to about 400 watts/m^2 (at the earth's surface). On the contrary, the upward directed longwave irradiance is around 350 watts/m^2 over most of the troposphere.

Figs. 12a-d illustrate the vertical distribution of the up and down radiative fluxes during the nighttime. The shortwave radiation of 270 watts/m^2 received at the 250 mb level is only a small fraction of that received during the daytime and it is depleted by less than 20 watts/m^2 by the 950 mb level. The upward directed shortwave radiation is nearly constant throughout the troposphere. By contrast the downward longwave radiation increases from about 100 watts/m^2 at the 250 mb level to about 400 watts at the surface, showing little day-night variation. The upward directed longwave radiation decreases from 360 watts/m^2 at the 950 mb level to 310 watts/m^2 at the 250 mb level.

During the daytime (around noon) the incoming radiation at the top of the atmosphere ($\approx$ 1100 watts/m^2) exceeds the total outgoing radiation ($\approx$ 650 watts/m^2). During the pre-sunrise hours the incoming radiation ($\approx$ 250 watts/m^2) is less than the total outgoing radiation ($\approx$ 400 watts/m^2). It is only when one integrates

over the 24 hour period that one sees that the net outgoing exceeds the incoming radiation.

The vertical distribution of the total and the short and longwave heating (or cooling) rates are shown in Figs. 13a-c for the two daytime and nighttime observations, respectively.

The low troposphere, below 500 mb, experiences a warming rate of about 4^{o} to 6^{o}C/day from the shortwave component in this region. The large heating rate is evidently due to the extreme dryness and to the presence of the deep dust layer. The longwave component shows that the cooling rate is also large, and increases with pressure. At 300 mb the cooling rate is 2^{o} to 4^{o}C/day while at 900 mb it is around 9^{o}C/day. The large cooling was noted for both of the daytime experiments (9 and 10 May 1979). The large cooling near the earth's surface results from the sharp drop in humidity in the surface layer and the very warm temperatures. The net radiation profile shows warming in the middle and upper troposphere. This warming is a consequence of the very effective shortwave warming of the dust layer.

The nighttime net radiative heating profile (shown in Fig. 13c) includes shortwave warming during the early morning hours. This warming however is very small being of the order of 1^{o}C/day. These observations are made around 6 a.m. local time when the ground temperature and the air temperature near the ground were close to their minimum value. Because of the lower temperature, the longwave radiation and its convergence were somewhat smaller at this time. The cooling rates in the troposphere below 600 mb were of the order of 4^{o}C/day. The net cooling was of the order of 2 to 3^{o}C/day and it affected mostly the atmosphere below 600 mb during the nighttime.

6.1 Thermodynamic Budget During the Afternoon Hours

The heat budget for the daytime observations is presented in Table 4. These are averages for the two days, 9 and 10 May. The horizontal advection brings in colder air into the domain (or warmer air out of the domain) over most of the troposphere. This accounts for the cooling rates of the order 1^{o} to 2^{o} in the mixed layer, while the strong cold advection is found just above the mixed layer. This cooling is consistent with the strong outflow in the anticyclonic circulation above the surface heat low. This outflow plays a key role in the removal of heat and the maintenance of the mixed layer potential temperature field. The lateral energy import, which is necessary for the maintenance of the stratification, occurs around 300 mb and perhaps also at higher levels of the upper troposphere. Here warm advection contributes significantly to the thermodynamic budget. This positive advection of heat at the upper levels is transmitted down to the lower levels by downward motions. In the very lowest troposphere below 900 mb weak advection (rate $\approx 0.2^{o}$C/day) is noted. Here the low level mass convergence brings in warm air from the hot desert to the south of the domain. Thus, in the afternoon hours the important aspects of lateral advection are a strong import of heat in the upper troposphere, an export in the lower troposphere and in the mixed layer and a smaller import in the lowest levels.

The computation of the horizontal advection terms shown in Table 4 (as well as in Table 5) was not very straightforward. The mean horizontal advection of

heat, term (2) in Eq. (11) for each layer, i, can be calculated directly from the wind (Section 5). This term also can be represented as:

$$[\vec{v}]_i \cdot [\vec{\nabla}\theta^*]_i = |[\vec{v}]|_i |[\vec{\nabla}\theta^*]|_i \cos \alpha_i \qquad (14)$$

where cos α is the angle between the two vector components and the vertical bars represent absolute magnitude. This term has been calculated for the intermediate levels, i + 1/2, by using a linear interpolation between layer i and i + 1 for each of the three quantities on the right hand side in Eq. (14). The values for term (2) are shown in column 2 in Tables 4 and 5, while those of the angle, α, are in column 6 and those of the product of the first two terms on the right hand side in Eq. (14), $|[v]\ [\nabla\theta^*]|$, are shown in column 7.

The role of the vertical advection appears to be more straightforward, it leads to a warming at all levels in the afternoon hours. The large warming occurs near the 600 mb level where the intensity of this warming is around 3°C/day. This largely counteracts the cooling from the lateral export in the middle levels.

The net radiative convergence leads to a warming over most of the middle troposphere between 800 and 400 mb. The warming rate is between 1 to 2°C/day. The largest warming occurs near 600 mb just around the top of the mixed layer and may be attributed to the shortwave warming of the dust layer which extended to about this altitude, as was noted in the direct measurements from the aircraft. Radiative cooling occurs in the very lowest troposphere, the strong cooling rate being around 5°C/day at the 950 mb level and is related to the sharp drop in the humidity above this level. The cooling comes from the divergence of the longwave irradiance. Cooling is again noted above 400 mb where the shortwave absorption is smaller. The sum of the advective and radiative changes is shown in Column 4 of Table 4.

The thermal imbalance among advective and radiative effects is large in the upper troposphere. However, above 500 mb there are a number of levels where α is around 90° and $|[v]\ [\nabla\theta^*]|$ is as large as 47 K/day. For these levels a small change in α can change the value of the mean horizontal advection of heat or even alter its sign. The magnitude and direction of $\vec{\nabla}\theta^*$ varies, depending on which of the three quantities, x, y, or θ, is the dependent variable in the multiple linear regression analyses. The cases tested showed that the angle α can vary by as much as $\pm$ 5° is x or y is the dependent variable, rather than θ. The value of α needed to give a thermal balance is called α_c and is shown in column 8. If α_c differs from α by less than 6°, it is reasonable to assume the radiative and advective terms summed in column 5 are in thermal balance as α is uncertain by $\pm$ 5°. Using this argument there is a thermal balance from 550 mb to 400 mb, but above 400 mb there is still a thermal imbalance with a net heating. It is safe to assume that subgrid scale heating by the convergence of eddy heat flux is small above the mixed layer (above 650 mb), thus this imbalance must largely reflect the local change of potential temperature over the upper troposphere. For the daytime flights we note a large positive imbalance of the order of 4 to 6°C/day in this region. This temperature change is consistent with the observed temperature change due to the slow arrival of an upper trough and southwesterly flows ahead of it. The observed warm advection is related to the warmer temperatures of this southerly component. The imbalances in the heat budget over the upper troposphere do not appear to be central to the maintainance of the heat low. Here the interesting region is below 650 mb.

It is reasonable to expect a balance by the convergence of eddy flux of heat below the top of the mixed layer. Thus the vertical profile of the convergence of eddy flux requires a cooling at 1000 mb, warming between 950 and 850 mb and very slight cooling between 800 and 700 mb. This is essentially consistent with the idea of vertical mixing and dry convective adjustment. However, it should be noted that the depth of the surface layer with superadiabatic lapse is extremely shallow, being of the order of a few hundred meters; thus convective adjustment would only require an overturning over a much shallower layer. The present calculations suggest that mixing is quite effective below 800 mb. Between 800 and 650 mb the magnitude of the eddy flux convergence is very small and even its sign may be questionable, since the error in this calculation can be as large as $\pm$ 0.5°C/day.

6.2 The Thermodynamic Budget During Night

The results of these calculations are illustrated in Table 5. The most striking aspect of the calculations is the essential reversal of the horizontal advection at several levels between day and night. At the low levels, below 800 mb, weak divergence and the nighttime strong radiative contributes to a weak cold advection, this implies that the outflowing air is in fact colder than its environment. This nocturnal reversal of the advection between the surface and 700 mb is consistent with the reversal of the vertical circulation cell between the heat-low region and its surroundings. At the middle troposphere we noted sinking motions and horizontal convergence. The converging air brings in relatively cold air from the surrounding regions. At these levels (450 to 550 mb) the rate of cooling is as large as 10°C/day during the nighttime.

This large cooling is entirely offset by the adiabatic warming resulting from the downward motions. The strongest adiabatic warming rate found near 500 mb has an intensity of 15°C/day. This is much stronger than the daytime estimates.

Radiative cooling prevails at all levels during the night. Its intensity lies between 1 to 3°C/day over most of the troposphere, cooling rates are largest in the upper troposphere where magnitudes between 4 to 8°C/day are encountered. The major difference in the net radiative field between day and night over this region is, of course, the absence of the shortwave component which contributes very significantly to a net warming during the daytime hours. The sum of the advective and radiative effects are shown in column 4 of Table 5. At all levels above 500 mb there is a thermal imbalance showing cooling. As was done in Section 6.1 the quantities α and α_c were calculated and are shown in columns 6 and 8, respectively. Even if α can vary by $\pm$ 5°, there remains a thermal imbalance among the radiative and advective terms summed in column 4 in Table 5. In the upper troposphere, near 300 mb, a large cooling rate of the order of 7°C/day is consistent with the synoptic scale cooling that was noted around this time as a cold trough approaching the region from the west on 12 May 1979. Between 850 and 600 mb an essential balance between the adiabatic warming and radiative cooling exists. The region below 850 mb is of considerable interest during the nighttime. The aircraft measurements of soil temperature over the desert during the nighttime flight shows temperatures of the order of 24.6°C, while the air temperature at the surface was close to 31°C. This implies a transfer of sensible heat from air to the land under a stable surface layer.

For balance, the planetary boundary layer experience a divergence of eddy flux of heat near 1000 mb and a convergence of flux above that level. The heat flux profiles for the day and night observations are shown in Fig. 14. Here the surface values of the fluxes were obtained by carrying out a surface heat budget calculation. The aircraft observations of the upward and downward fluxes and the soil temperature measurements were used to determine the heat flux at the lower boundary. In the lowest kilometer, the eddy flux of heat is directed up during the day and downward during the night. It has been shown in Krishnamurti (1979) that the stabilizing of the mixed layer requires that $\partial^2[\omega^*\theta^*]/\partial p^2$ be positive. The profiles of $[\omega^*\theta^*]$ shown in Fig. 10 are extremely interesting in this regard. During the nighttime $\partial^2[\omega^*\theta^*]/\partial p^2 < 0$ and contributes to a destabilization of the mixed layer. This becomes more apparent when we note that in its absence there is in fact a strong stabilization by the advective and radiative processes. It thus seems that the stable boundary layer requires a destabilization by the eddy heat flux convergence even though the flux is directed downwards. During the daytime the second derivative of the eddy heat flux (Fig. 14) appears quite small in the lowest kilometer. Between 700 and 925 mb the eddy heat flux is directed downward and the profile contributes to a destabilization. On the other hand, radiative warming of the dust layer and the strong radiative cooling of the surface layer act to stabilize the sounding. Thus, the deep-mixed layer over the desert has a strong destabilization by the convective processes. The strong sensible heat flux at the ground, $([-\omega^*\theta^*])_{1000}$, is carried up to about 925 mb beyond which the eddies transport heat downwards. One can think of two effective heating layers, one at the ground and one in the dust layer above 800 mb. The region between the ground and 800 mb experiences warming from the convergence of eddy flux, while the region above 800 mb is cooled from the divergence of eddy flux which is increasing downwards. This role of eddy flux is quite different from that which one is accustomed to in the formulation of dry convective adjustment. The apparent difference is due to the role of the dust in the radiative heat balance.

7. Concluding Remarks

A unique set of observations was provided by the GARP Monsoon experiment for studies of the heat low over the Saudi Arabian desert. The experiment provided a dense network of upper air observations (including measurements of temperature, humidity, pressure and winds). In addition, the research aircraft provided profiles of short and longwave irradiances, measurements of soil temperature, surface albedo, and aerosol characteristics, especially in the dust layer.

The major findings of the present study are:

- A well-mixed layer with near constancy of potential temperature and specific humidity is found from the surface up to 650 mb during the afternoon hours over the desert heat low. During the nighttime, strong surface cooling results in the establishment of stable conditions from the surface up.

- Calculations of vertical motion and horizontal divergence show that downward motions prevail from about 1 km through the depth of the troposphere in the afternoon hours. Weak ascending motions are found in the lowest kilometer. During the night, downward motions extend to the ground. Weak surface convergence in the heat low is capped by a region of low level horizontal divergence near the 850 -

700 mb levels. Another region of convergence is found near the upper troposphere. During the night, the low level convergence in the heat low is replaced by a weak field of horizontal divergence.

The various terms of the hydrodynamic budget were evaluated over the region of heat low and many interesting results emerged from these balances:

- Longwave radiative cooling of the order of 4 to 6^{o}C/day prevails throughout the troposphere, an exception being the very warm surface layer during daytime where exceptionally large cooling occurs as a consequence of the warm temperature and the strong drying of the air in the vertical direction. The surprising element of the solar radiation measurements is the very strong warming rates, which during the daytime exceed the longwave cooling rates by a couple of degrees over most of the troposphere. This is attributed to the strong absorption of shortwave radiation in the dust layer which extends to 650 mb. Thus, an important element in the thermal balance of the mixed layer is the net radiative warming, which decreases with increasing pressure and contributes to stabilization of the mixed layer.

- Downward motions contribute to warming during daytime as well as nighttime hours. Largest descent occurs in the middle levels, thus it has a role in stabilizing the mixed layer as well. The stabilization by large scale divergence is determined by a covariance of the dry static stability and the divergence. In the region of the superadiabatic lapse rate next to the ground some convergence exists in the daytime; here also the covariance contributes to stabilization.

- The neutral lapse rate of the mixed layer during the daytime is maintained by a destabilization from the vertical eddy heat flux convergence. Its profile has been calculated from the thermodynamic budget and has been shown to destablize during the day and stabilize during the night. During the daytime, the warm desert surface is a source of heating for the lower troposphere. The sensible heat flux is carried upward by the eddies in the unstable planetary boundary layer. The shortwave warming of the dust layer in the upper part of the mixed layer also acts as another source of heating over this region. This results in a downward eddy heat flux below 700 mb. The presence of dust provides a unique destabilizing effect from the convergence of eddy flux, by heating below 800 mb and cooling above.

- A net radiative heat loss at the top of the atmosphere during the 24 hour period over the region of the heat low requires that energy be supplied to this region for the maintenance of stratification. Here the thermal budget calculations provide an important insight. We find that this import of heat occurs in the upper troposphere during both day and night. This is the region where energy is imported and transmitted to the lower levels via vertical advection.

The heat low is a shallow, cyclonic, warm low pressure area in the lowest kilometer of the atmosphere. A strong anticyclonic outflow is already evident at 850 mb and is fairly pronounced at the 700 mb level. An important question that is frequently asked is: "Why downward motions exist well above this anticyclonic outflow layer?" The downward motions go in hand with mass convergence and energy supply in the upper troposphere; they go in hand with the drying of the troposphere which in turn provides the strong radiative forcing. We believe that the downward motions are in fact part of a large scale vertical overturning which is asociated with the Hadley and east-west circulations. These circulations

tend to favor regions of the large surface albedo for their descent. The desert regions of the subtropics provide such a lower boundary. Evidence for the large scale extent of the upper circulations may be seen in the divergent wind for the 9, 10, 11, and 12 May 1979. This average circulation is shown in Fig. 15 which shows the lateral coupling between the ascending motions over the convective region of the monsoons and the desert area of Saudi Arabia where the descending motions of the east-west overturning are occurring.

Numerical simulation of the detailed kinematic and thermodynamic structure of the heat low is an important unsolved problem. A small computational domain enclosing the high surface albedo region may not be adequate for such a modeling effort, since the supply of energy in the upper troposphere and the descending motion over the deep troposphere have to be modeled. This may require a large domain that includes the region of the compensating upward motion which may be the intertropical convergence zone many thousands of miles away.

8. REFERENCES

Ackerman, S. A., and S. K. Cox, 1982: The Saudi Arabian heat low, aerosol distribution, and thermodynamic structure. To appear in J. Geophys. Res.

Charney, J. G., 1975: Dynamics of deserts and drought in the Sahara. Quart. J. Roy. Meteor. Soc., 101, 193-202.

Krishnamurti, T. N., 1979: Tropical Meteorology, Report No. 364. Available from the World Meteorological Organization, 1211 Geneva 20, Switzerland, 428 pp.

Smith, E. A., S. A. Ackerman, S. K. Cox, and T. H. Vonder Haar, 1980: Summer MONEX High Altitude Aircraft Radiation Measurements, Dept. of Atmospheric Science Report for NSF Grant No. NSF ATM/78-0235. Available from Colorado State University, Fort Collins, CO 80523, 89 pp.

Summer MONEX Field Phase Report, 1981: First GARP Global Experiment Operations Report Series, vol. 8. Prepared by the International MONEX Management Centre (Summer), New Delhi. Available from the World Meteorological Organization, 1211 Geneva 20, Switzerland, 315 pp.

Table 1. LIST OF ACRONYMS

MONEX	MONsoon EXperiment
NASA	National Aeronautics and Space Administration
CV990	CONVAIR 990 (4 engine jet)
TIROS	Television Infra-Red Observation Satellite
GARP	Global Atmospheric Research Programme

Table 2. NUMBER OF WIND OBSERVATIONS IN EACH LAYER

LAYER (mb)	Day (May 9)	Day (May 10)	Day (Night) (May 12)
200-300	34	48	30 (5)
300-400	55	57	41 (15)
400-500	57	53	51 (17)
500-600	46	59	47 (16)
600-700	52	49	34 (23)
700-800	45	43	29 (12)
800-900	35	35	28 (12)
900-1000	25	40	20 (15)

Note: Nighttime only observations are shown within parentheses.

Table 3. LIST OF USEFUL SYMBOLS

Symbol	Meaning of symbol
a,b,c	coefficients of the linear regression for the east-west wind
d,e,f	coefficients of the linear regression for the north-south wind
c_p	specific heat at constant pressure
F_{iU}	upward irradiance for long and short waves
F_{iD}	downward irradiance for long and short waves
g	acceleration of gravity
ΣH_j	heat sources and sinks
p	pressure
p_0	reference pressure = 1000 mb
R	gas constant
T_L	net longwave radiative heating rate
T_S	net shortwave radiative heating rate
t	time
u	east-west wind component
v	north-south wind component
$\vec{v}$	horizontal wind vector
θ	potential temperature
ω	vertical p-velocity
$\omega^*\theta^*$	eddy heat flux
∇	horizontal vector gradient operator
ε, α, β	correction factors for the horizontal divergence
[ ]	area average
*	departure from area average

Table 4. THERMODYNAMIC HEAT BUDGET DURING AFTERNOON HOURS

Pressure mb	$-[\vec{v}] \cdot [\vec{\nabla}\theta]$ K/day	$-[\omega]\frac{\partial[\theta]}{\partial p}$ K/day	$[\Sigma H_i]$ K/day	Σ K/day	α Deg	$\lvert\vec{v}\rvert \lvert\vec{\nabla}\theta^*\rvert$ K/day	α_c Deg
1000				+8.4			
950	+0.2	+0.3	-5.1	-4.6	114	0.6	-
900	-0.6	+0.7	-4.2	-4.1	64	1.2	-
850	-2.1	+0.1	-1.5	-3.5	14	2.2	-
800	-1.7	+0.9	+0.9	+0.1	40	2.1	-
750	-1.2	+0.8	+0.8	+0.4	66	2.0	26
700	-1.2	+0.9	+0.5	+0.2	71	3.3	55
650	-1.0	+2.1	+1.1	+2.2	75	4.1	37
600	-2.6	+3.0	+2.4	+2.8	73	9.6	55
550	-5.1	+2.8	+2.3	+0.0	70	16.7	70
500	-4.0	+2.5	+2.4	+0.9	76	19.0	73
450	-2.4	+2.0	+2.3	+1.9	82	21.2	77
400	+0.5	+1.4	+0.6	+2.5	91	26.6	86
350	+4.3	+1.0	-0.8	+4.5	100	32.4	90
300	+6.4	+0.6	-1.8	+5.2	98	47.0	91

Table 5. THERMODYNAMIC HEAT BUDGET DURING NIGHTTIME HOURS

Pressure mb	$-[\vec{v}] \cdot [\vec{\nabla}\theta]$ K/day	$-[\omega]\frac{\partial[\theta]}{\partial p}$ K/day	$[\Sigma H_i]$ K/day	Σ K/day	α Deg	$\lvert\vec{v}\rvert \lvert\vec{\nabla}\theta^*\rvert$ K/day	α_c Deg
1000				+2.0			
950	-1.4	+0.4	-1.7	-2.7	21	1.5	-
900	-0.3	+0.8	-2.1	-1.6	53	0.6	-
850	-0.0	+1.7	-2.1	-0.5	84	0.1	-
800	+0.1	+1.3	-1.6	-0.2	97	0.4	-
750	+0.4	+1.6	-1.7	+0.3	110	1.2	-
700	+0.1	+1.9	-2.4	-0.4	93	2.2	-
650	-0.9	+4.6	-3.8	-0.1	75	3.6	77
600	-4.4	+8.1	-3.7	0.0	56	7.9	56
550	-10.6	+11.7	-1.6	-0.5	37	13.3	41
500	-11.8	+15.4	-2.9	+0.7	47	17.1	43
450	-11.8	+9.6	-1.3	-3.5	56	21.1	67
400	-9.7	+5.1	-2.4	-7.0	67	24.6	84
350	-5.9	+2.6	-4.6	-7.9	78	27.7	94
300	-1.3	+0.8	-6.7	-7.2	88	44.6	98

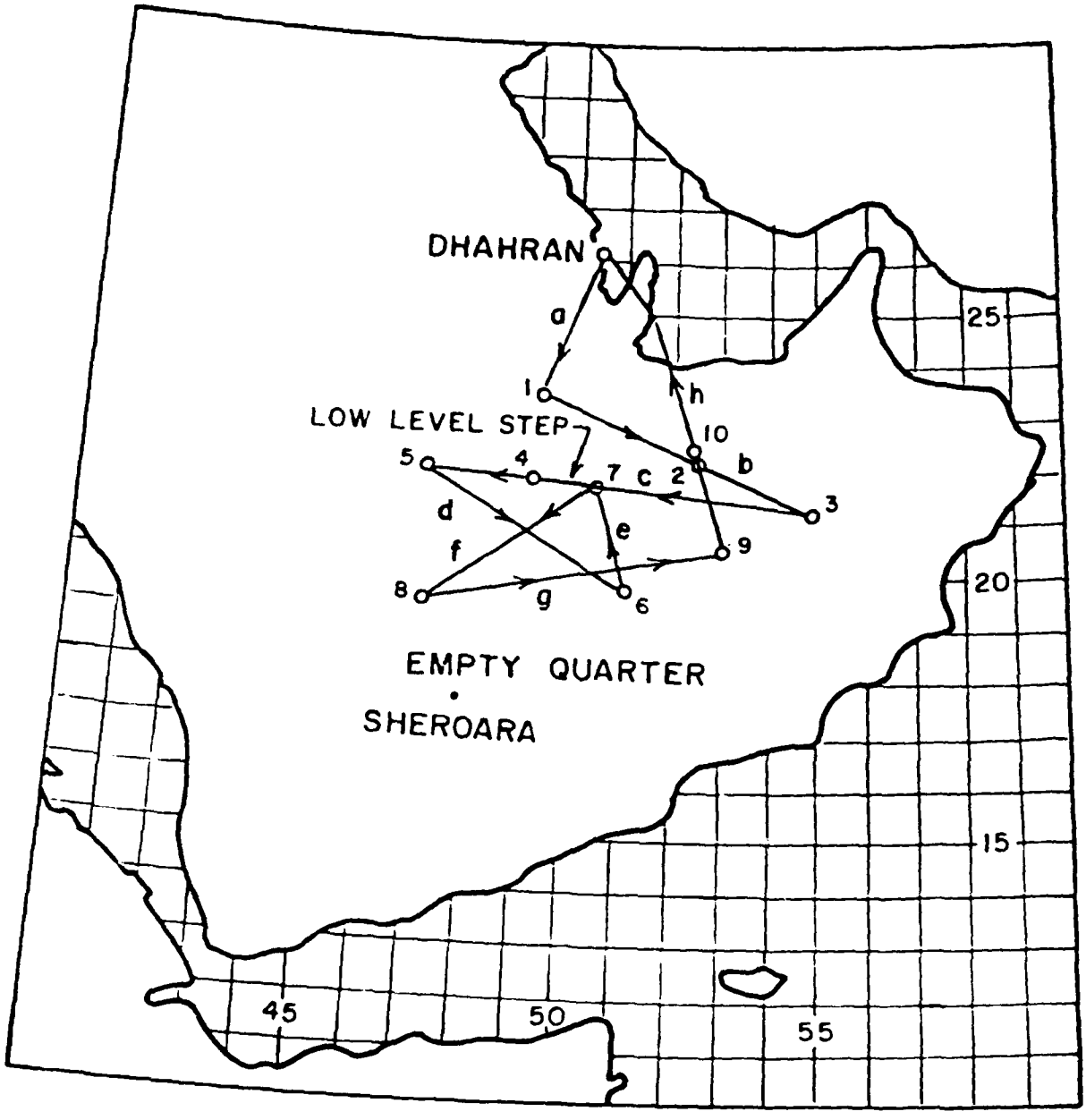

Figure 1. The flight path of CV990 near the Empty Quarter in Saudi Arabia. The numbers indicate the order in which the dropsondes were deployed.

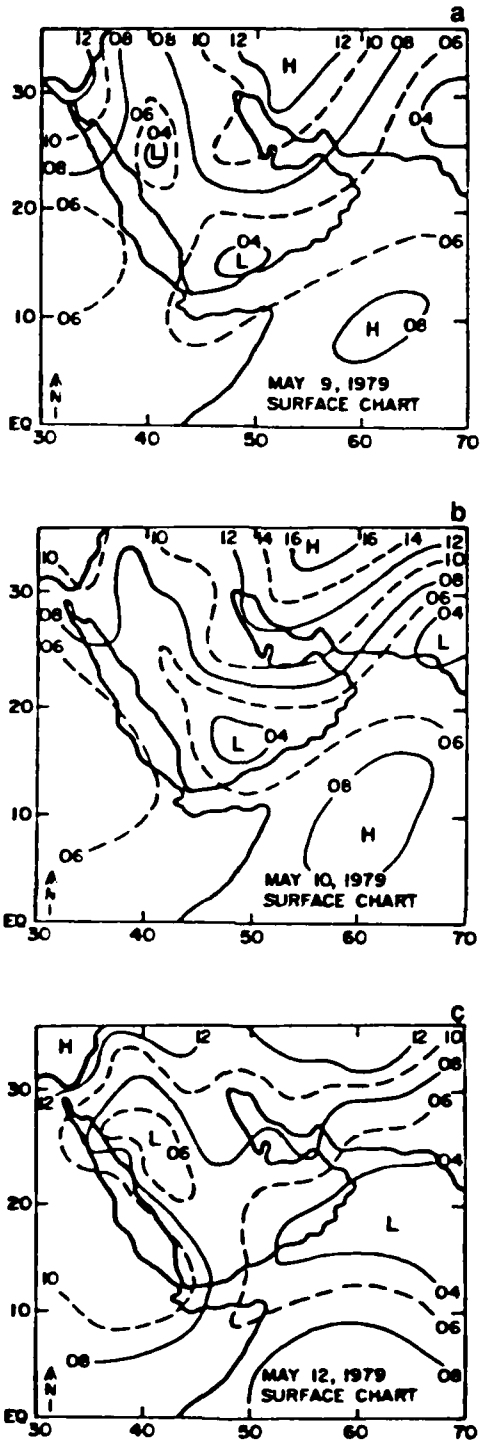

Figure 2. Surface analysis over Saudi Arabia for 9, 10, and 12 May 1979, 00Z, respectively. Isopleths show a level pressure (departure from 1000 mb).

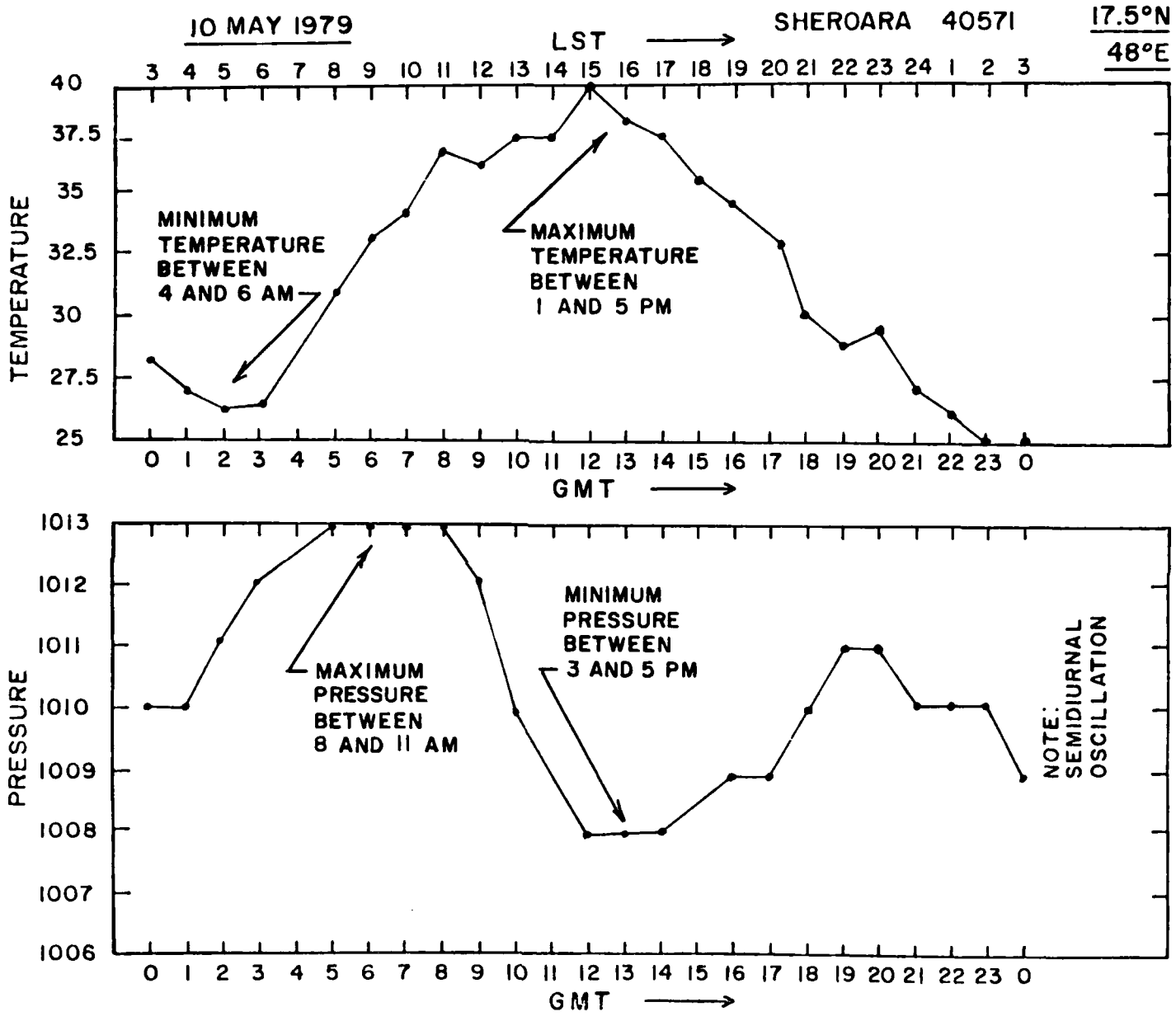

Figure 3. Surface pressure and temperature as a function of time at Sheroara on 10 May 1979. This illustrates the diurnal variation.

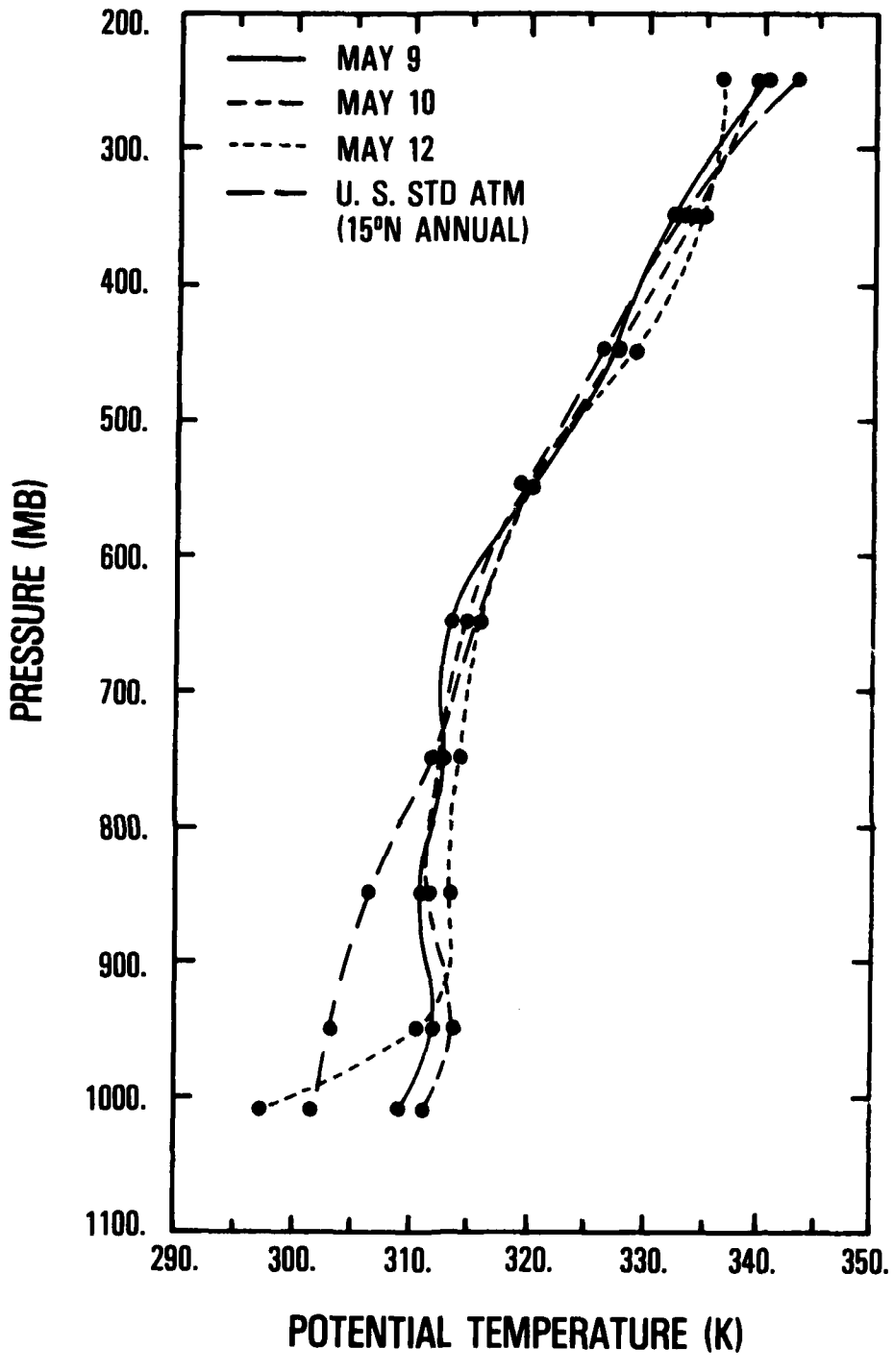

Figure 4. Mean vertical potential temperature profile for the three missions on 9, 10, and 12 May. Also shown here is potential temperature profile of the U.S. Standard Atmosphere at 15°N.

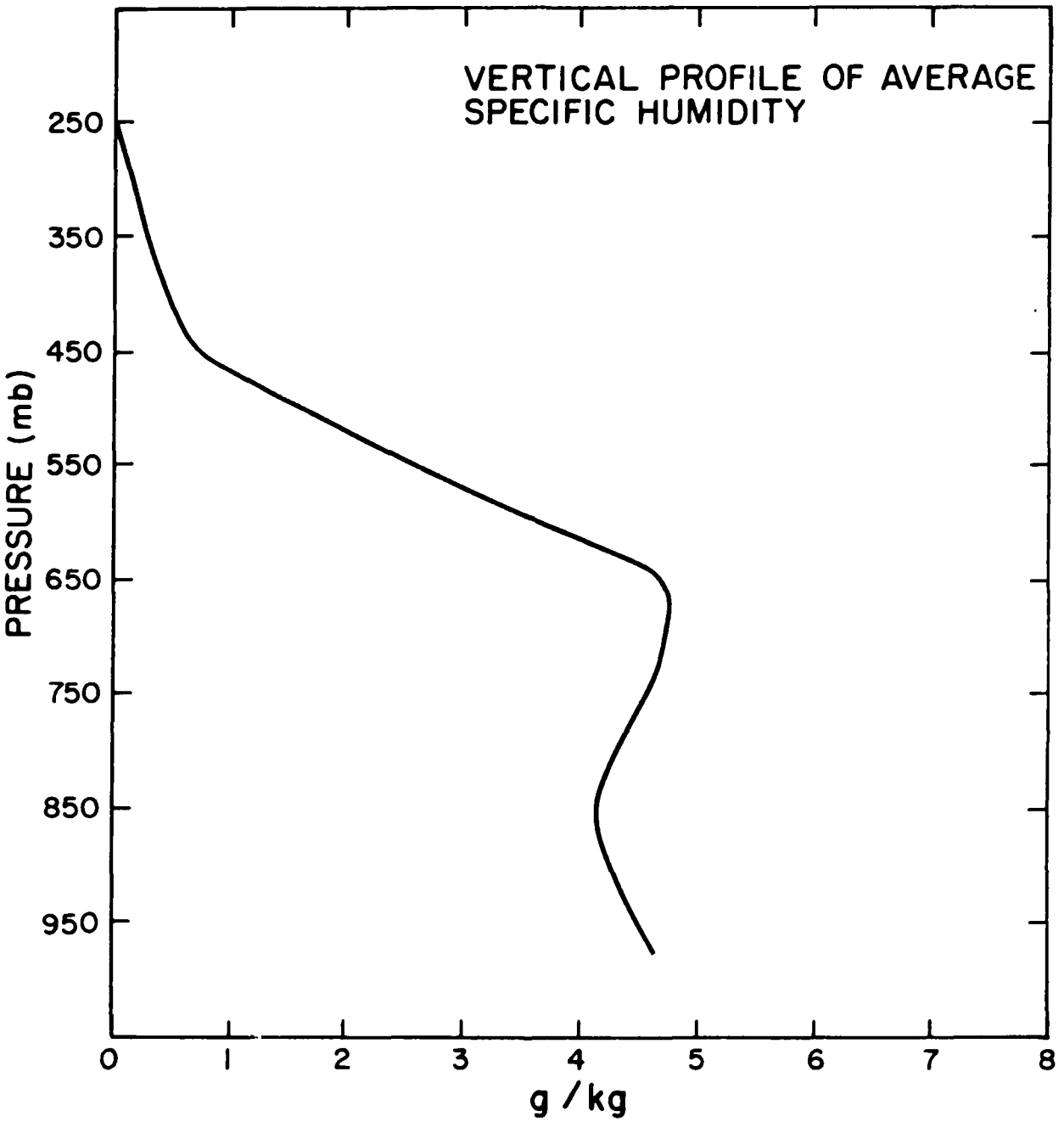

Figure 5. Vertical profile of the average specific humidity (g/kg) averaged for the two daytime missions.

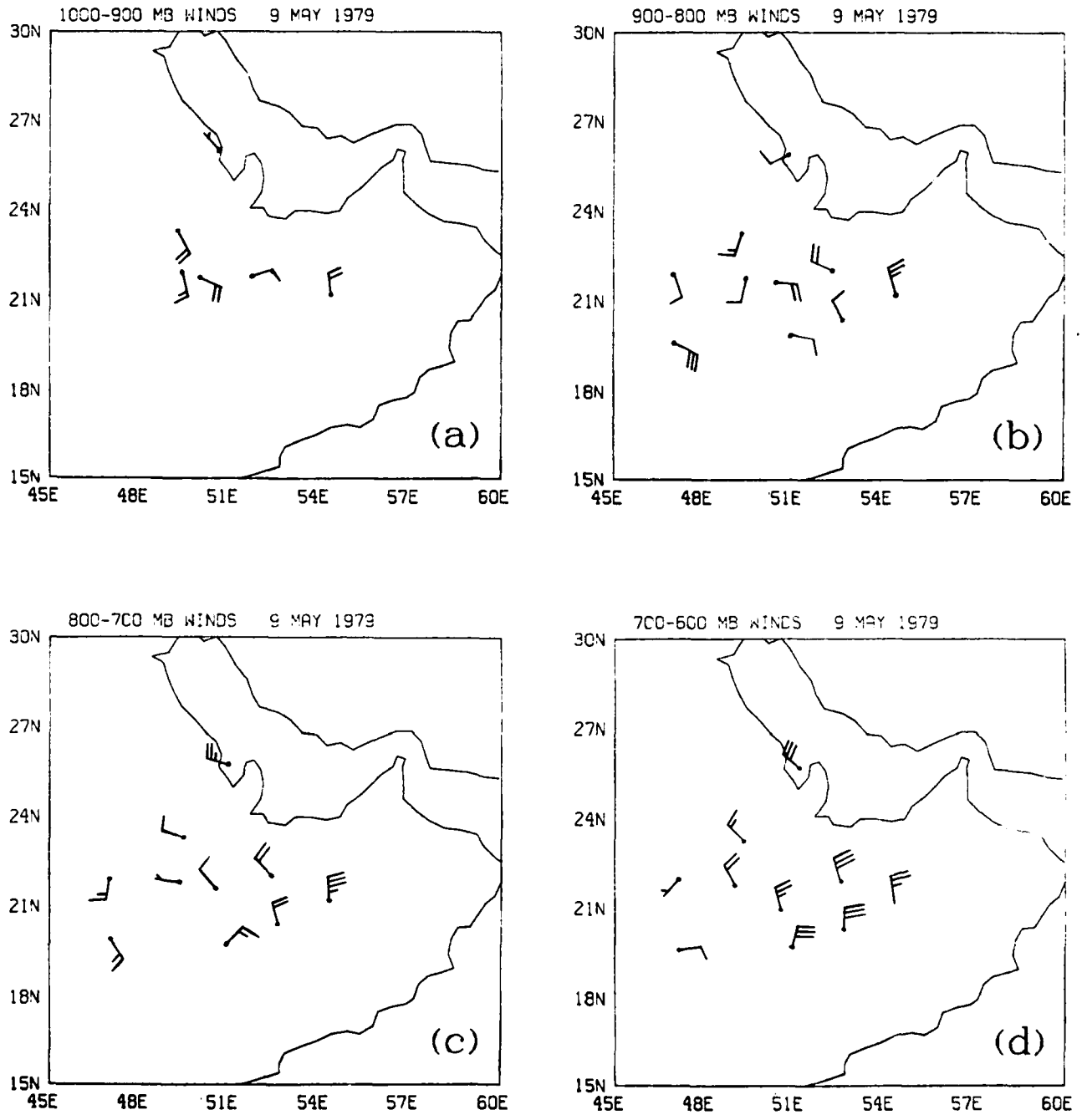

Figure 6 (a-d). Mean direction and speed of the horizontal winds at various altitudes for various locations over Saudi Arabia for 9 May 1979. Pressure levels are indicated at the top of the panels.

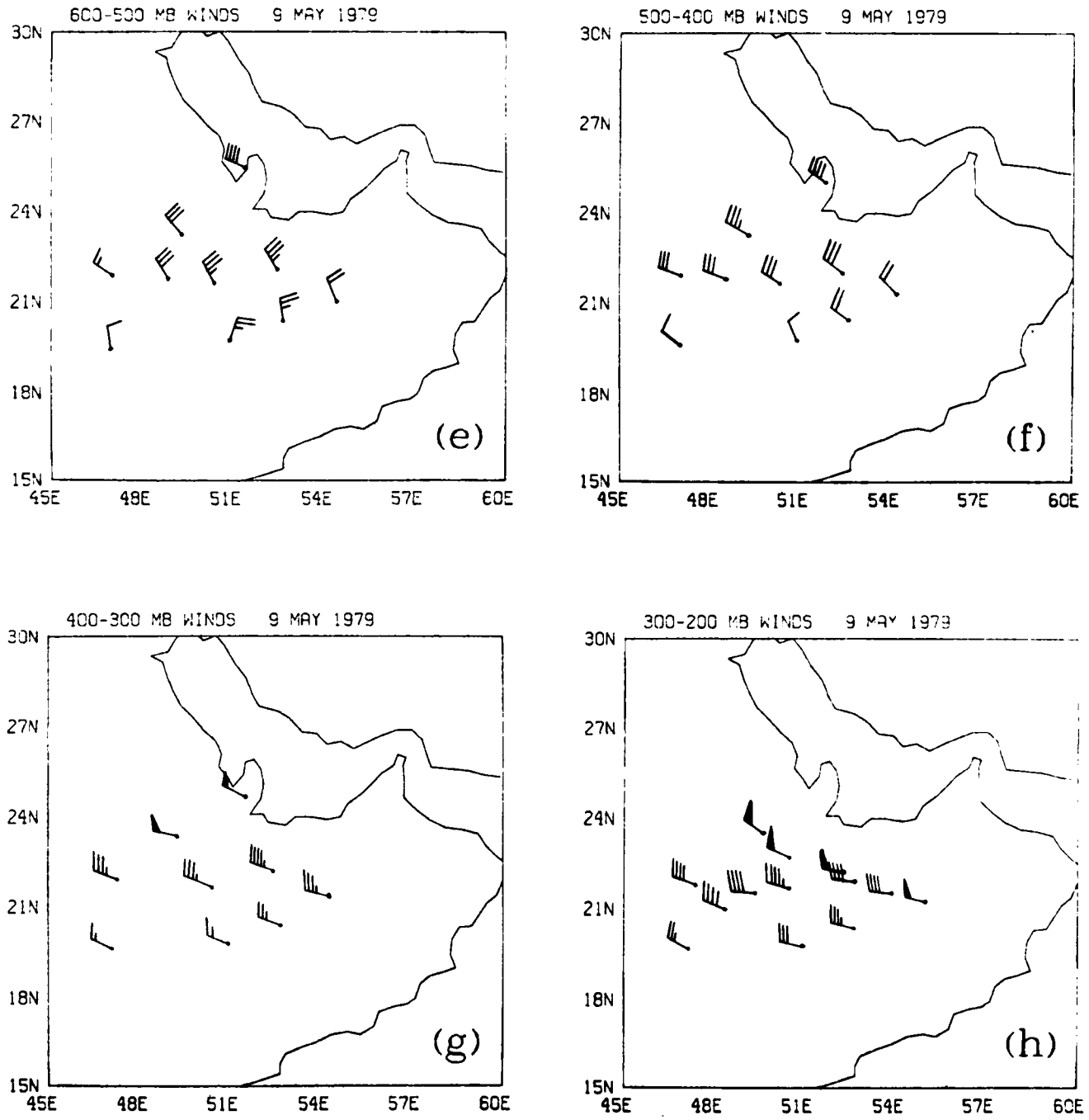

Figure 6 (e-h). Mean direction and speed of the horizontal winds at various altitudes for various locations over Saudi Arabia for 9 May 1979. Pressure levels are indicated at the top of the panels.

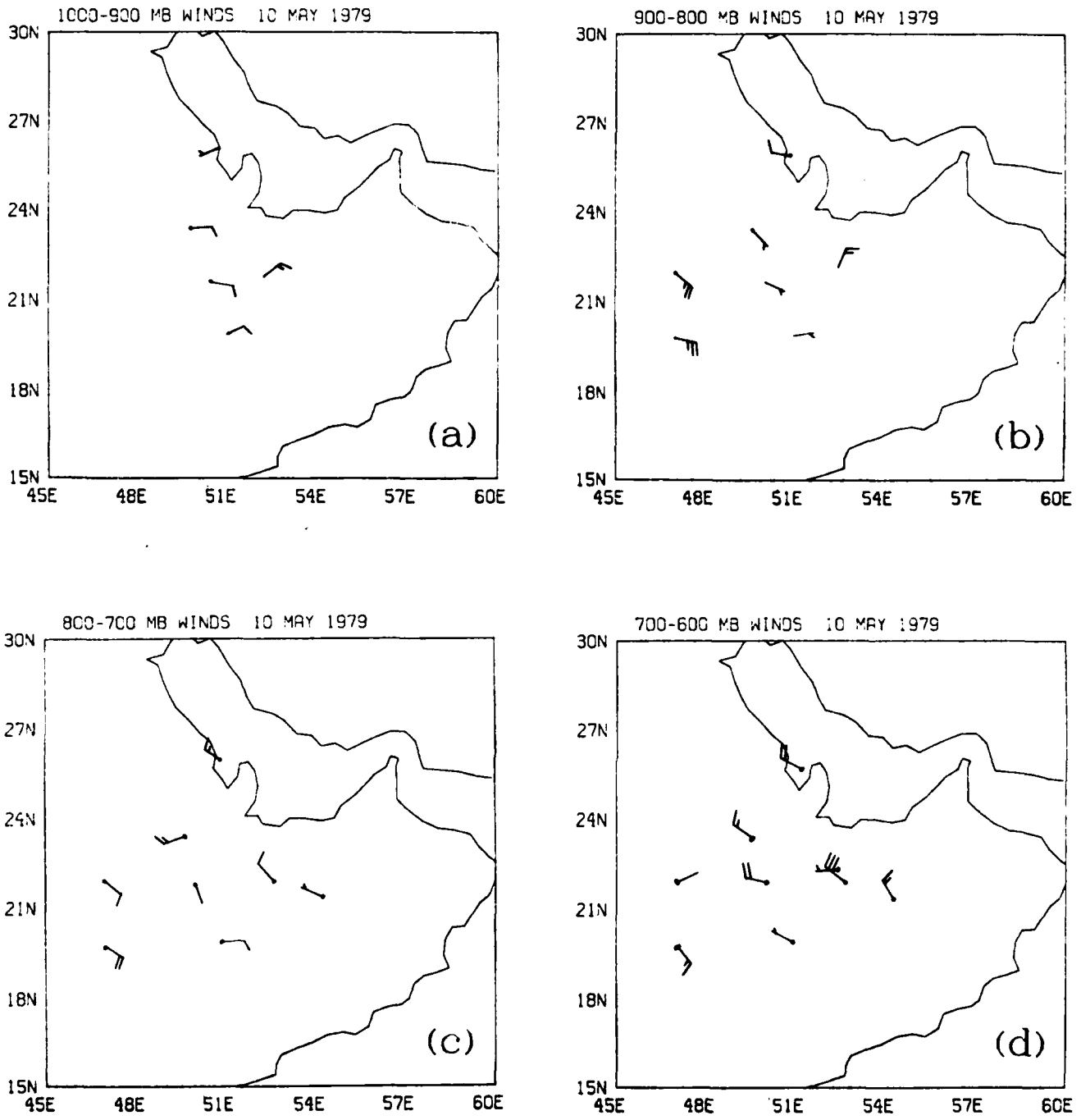

Figure 7 (a-d). *Mean direction and speed of the horizontal winds at various altitudes for various locations over Saudi Arabia for 10 May 1979. Pressure levels are indicated at the top of the panels.*

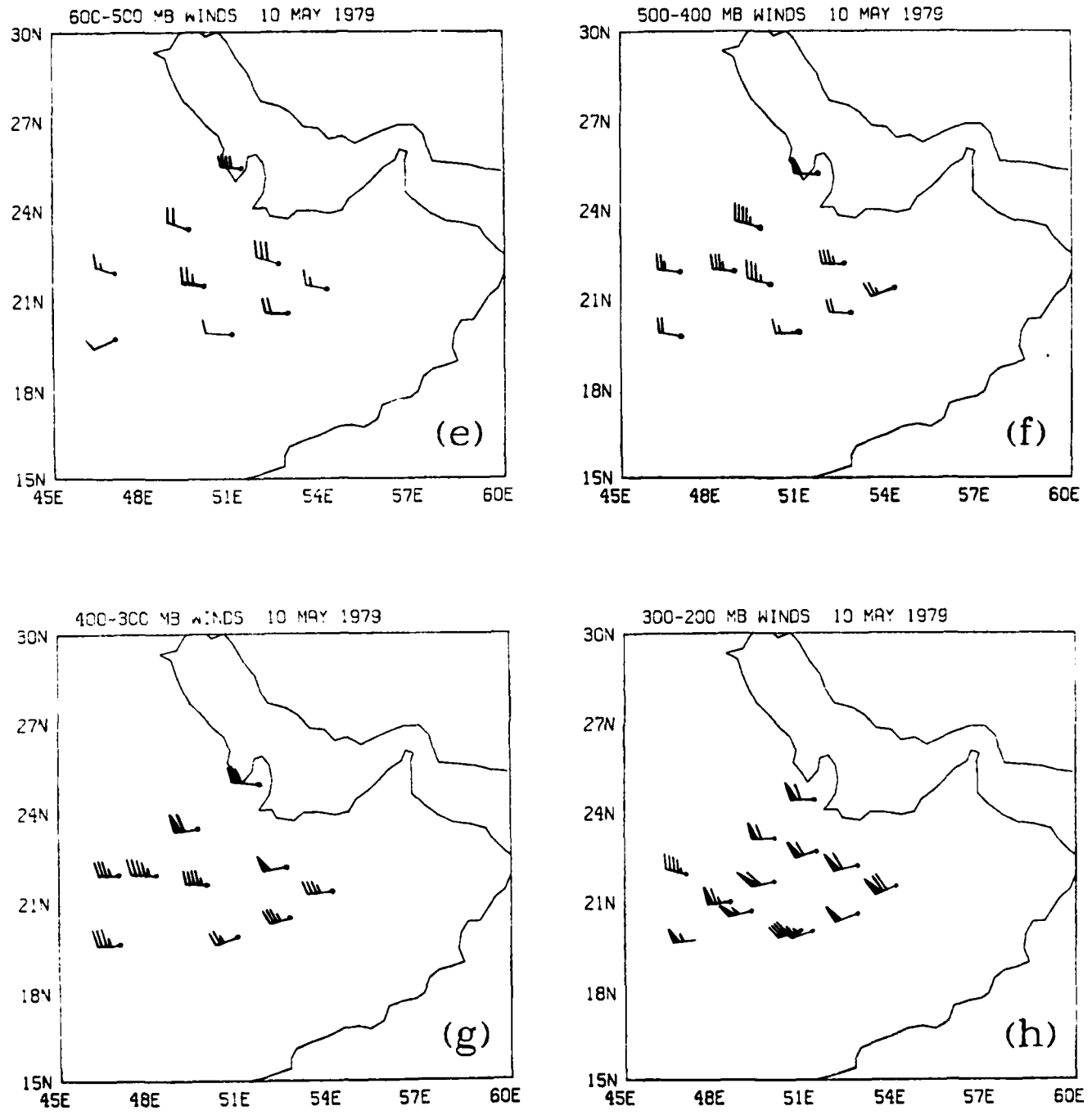

Figure 7 (e-h). Mean direction and speed of the horizontal winds at various altitudes for various locations over Saudi Arabia for 10 May 1979. Pressure levels are indicated at the top of the panels.

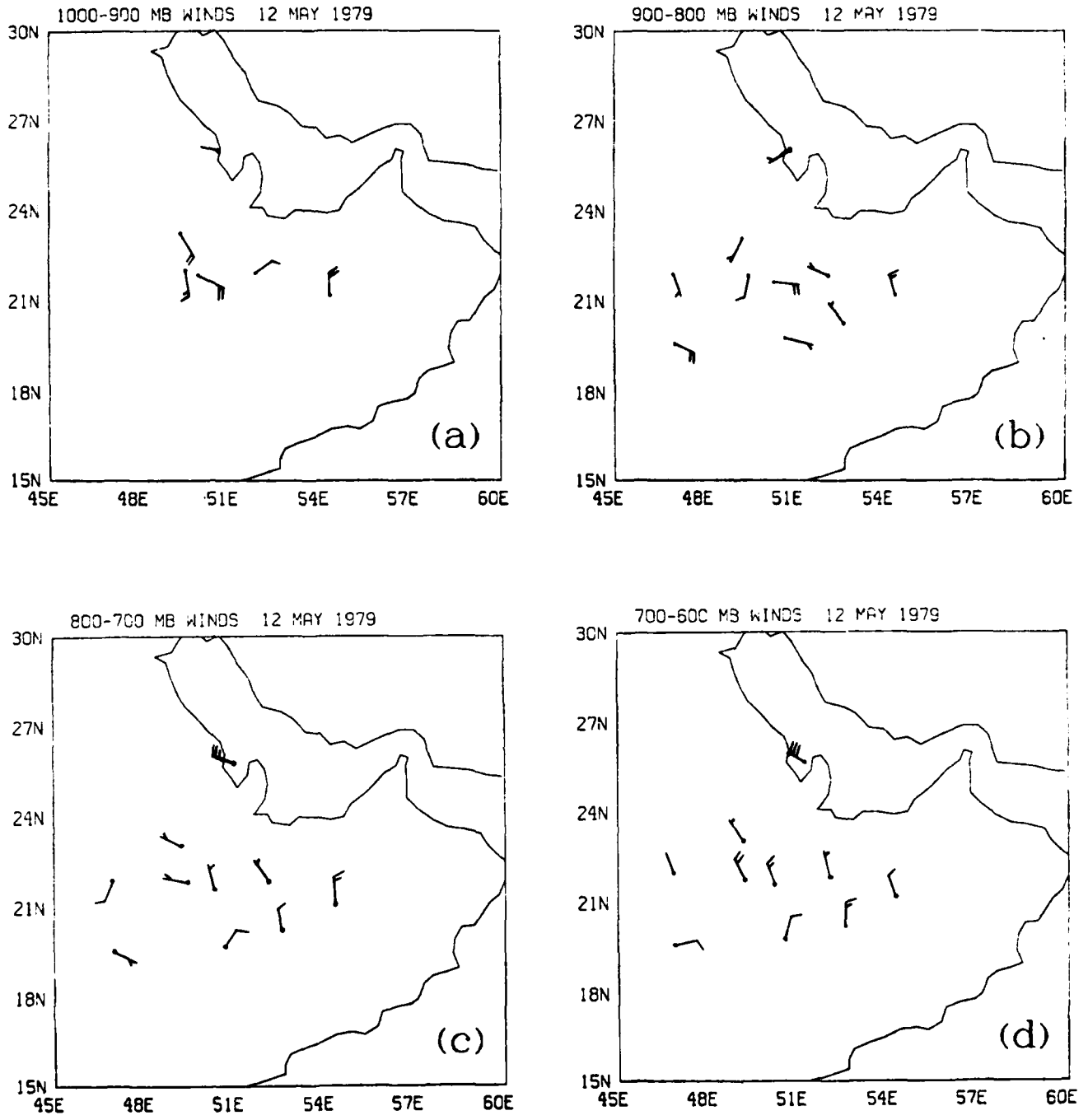

Figure 8 (a-d). Mean direction and speed of the horizontal winds at various altitudes for various locations over Saudi Arabia for 12 May 1979. Pressure levels are indicated at the top of the panels.

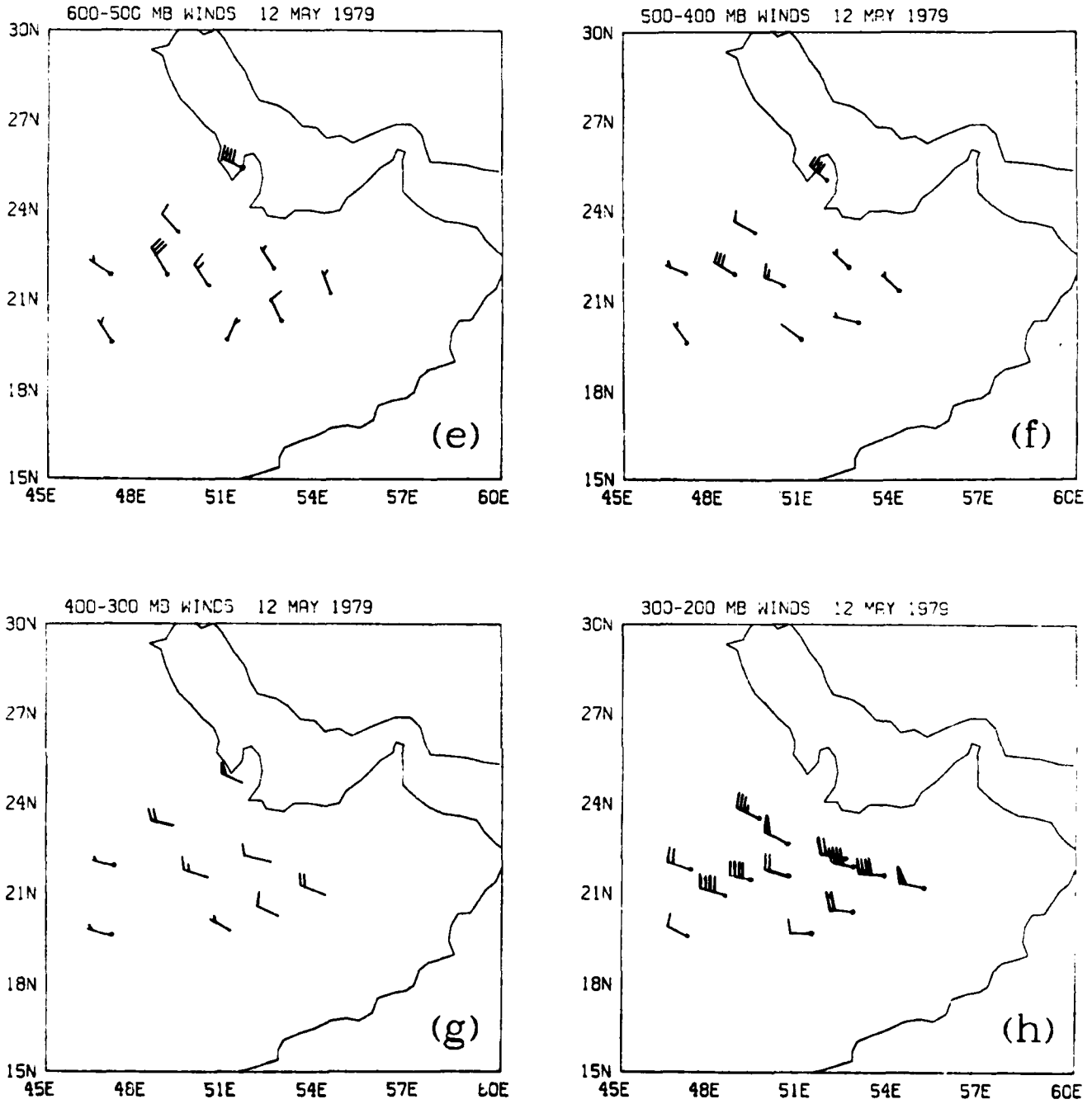

Figure 8 (e-h). Mean direction and speed of the horizontal winds at various altitudes for various locations over Saudi Arabia for 12 May 1979. Pressure levels are indicated at the top of the panels.

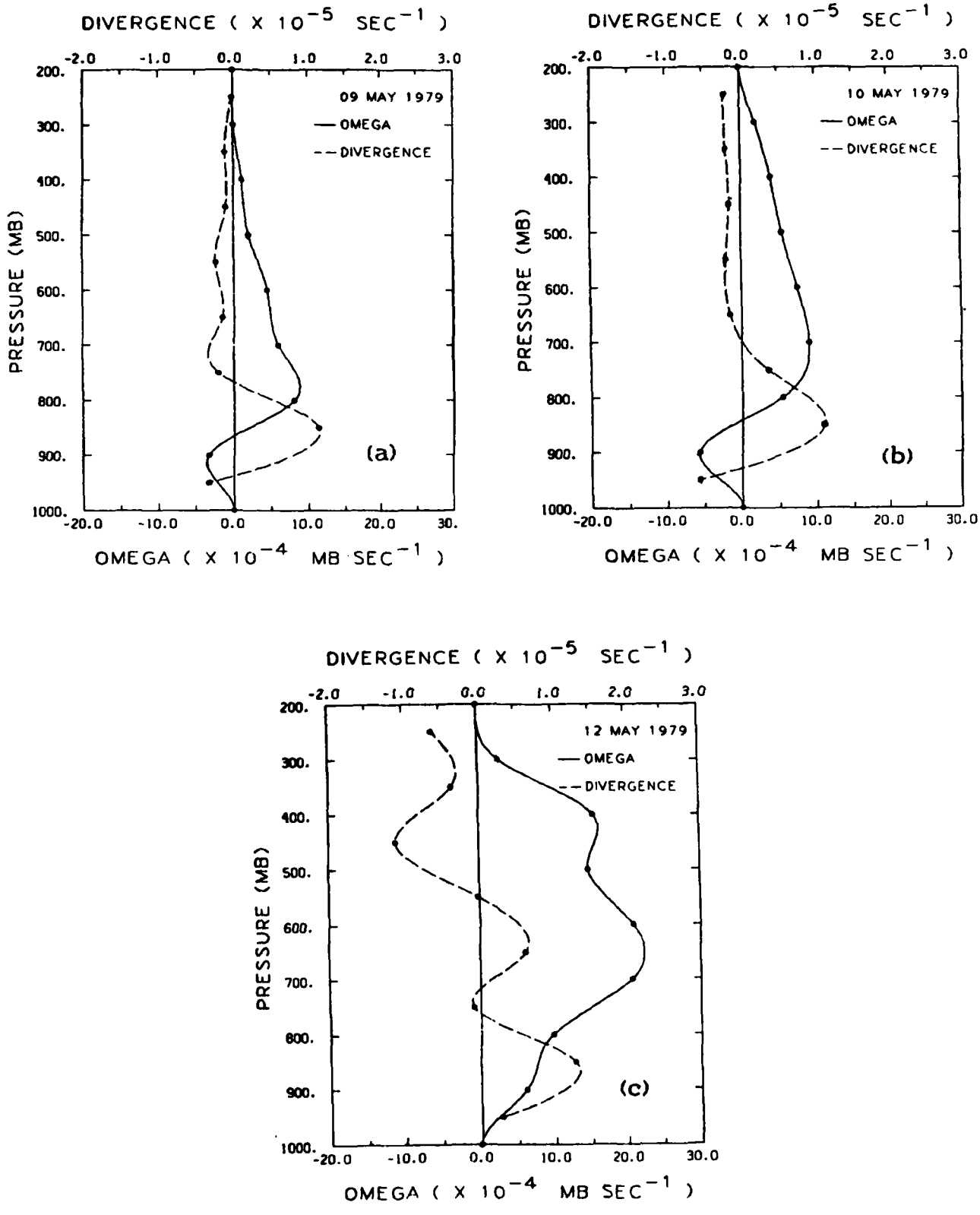

Figure 9 (a-c). Mean horizontal divergence and vertical motions for 9, 10, and 12 May, respectively.

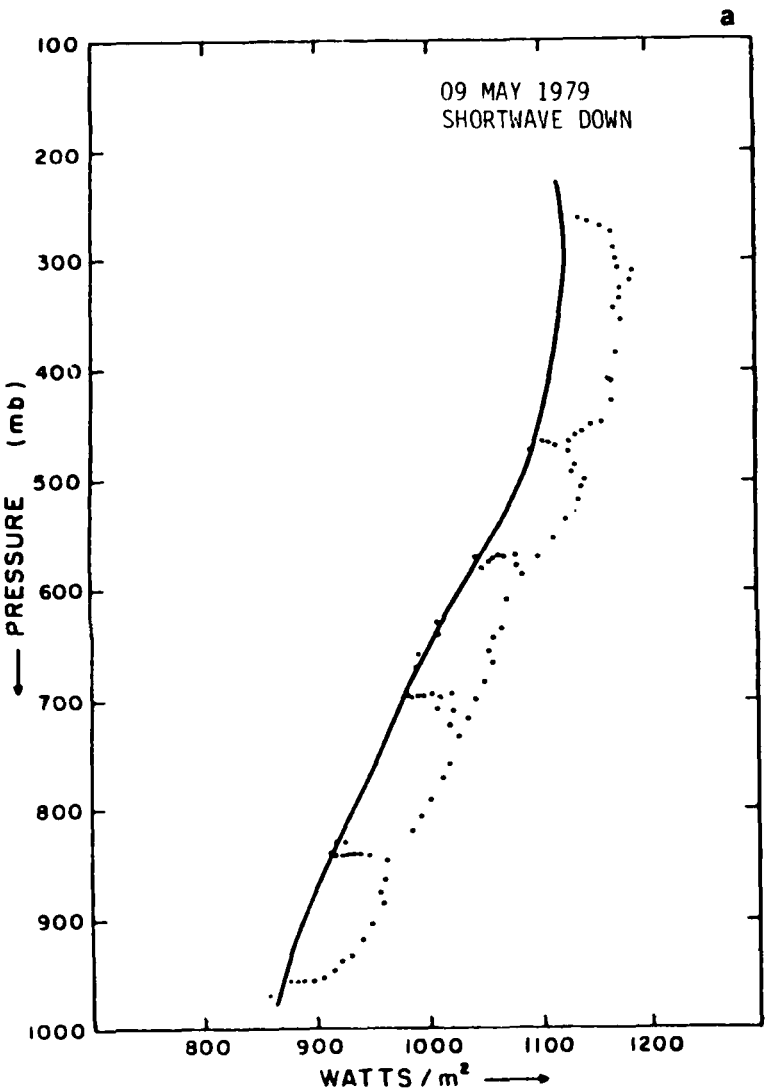

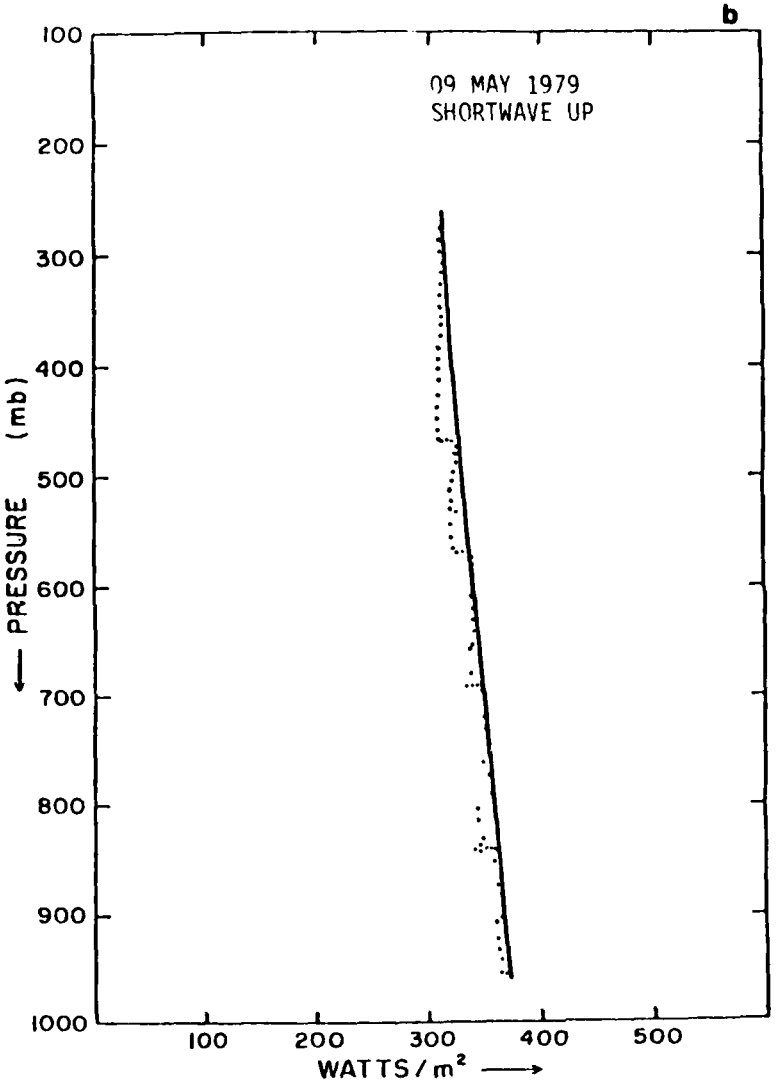

Figure 10 (a,b). Upward and downward shortwave irradiance measurements on 9 May plotted as a function of pressure. Units in watts/m^2.

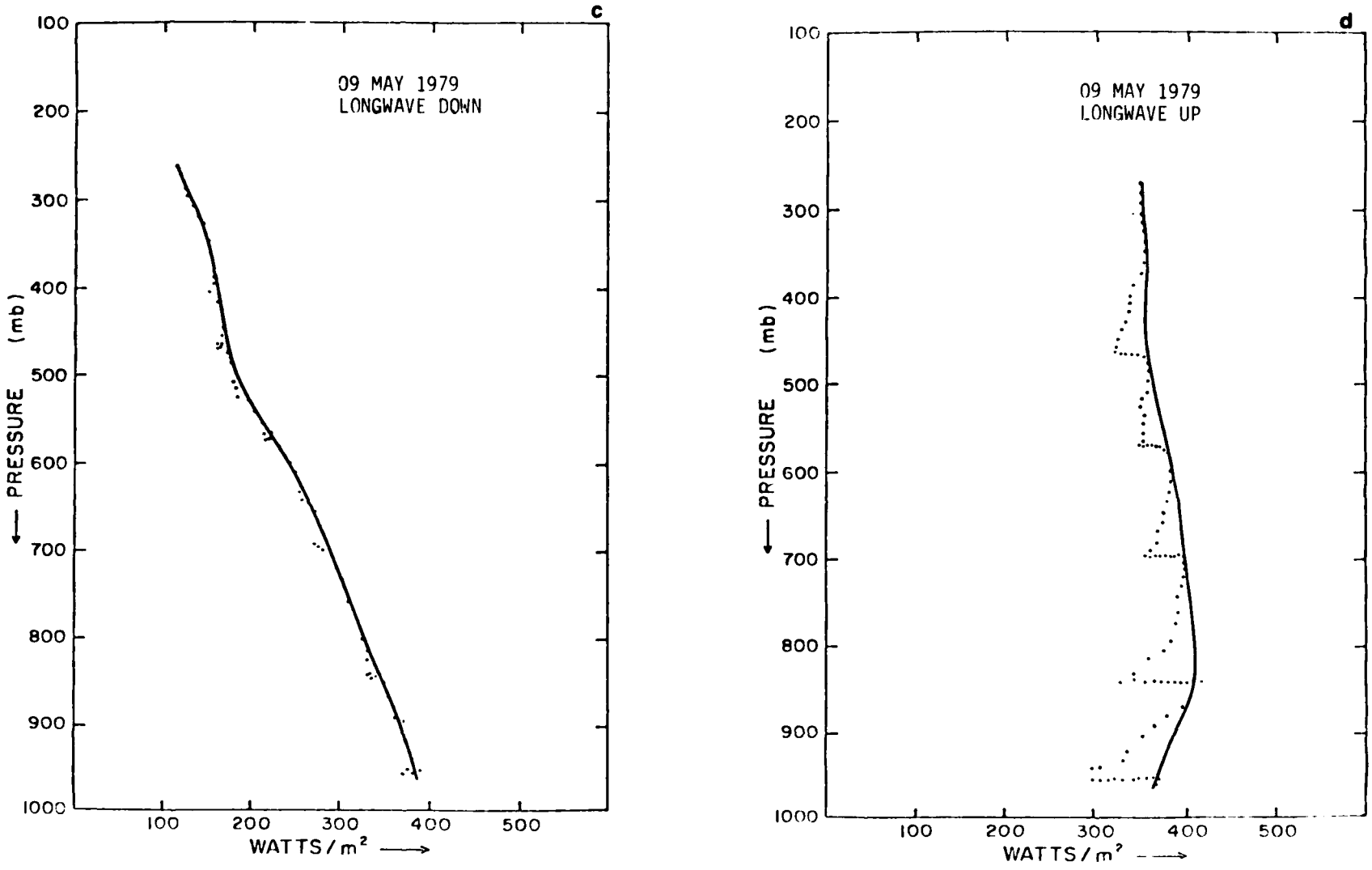

Figure 10 (c,d). Upward and downward longwave irradiance measurements on 9 May plotted as a function of pressure. Units in watts/m^2.

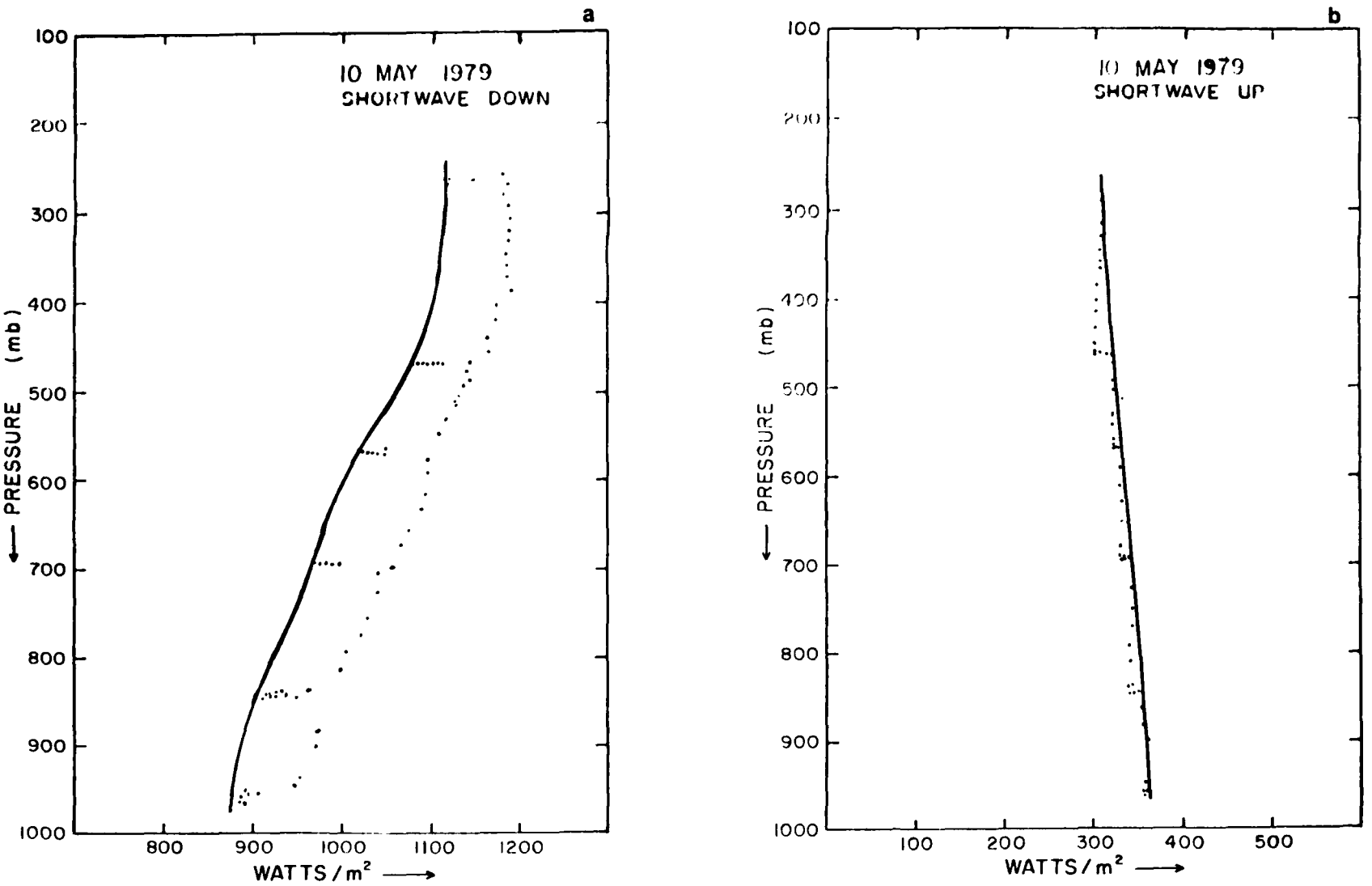

Figure 11 (a,b). Upward and downward shortwave irradiance measurements on 10 May plotted as a function of pressure. Units in watts/m^2.

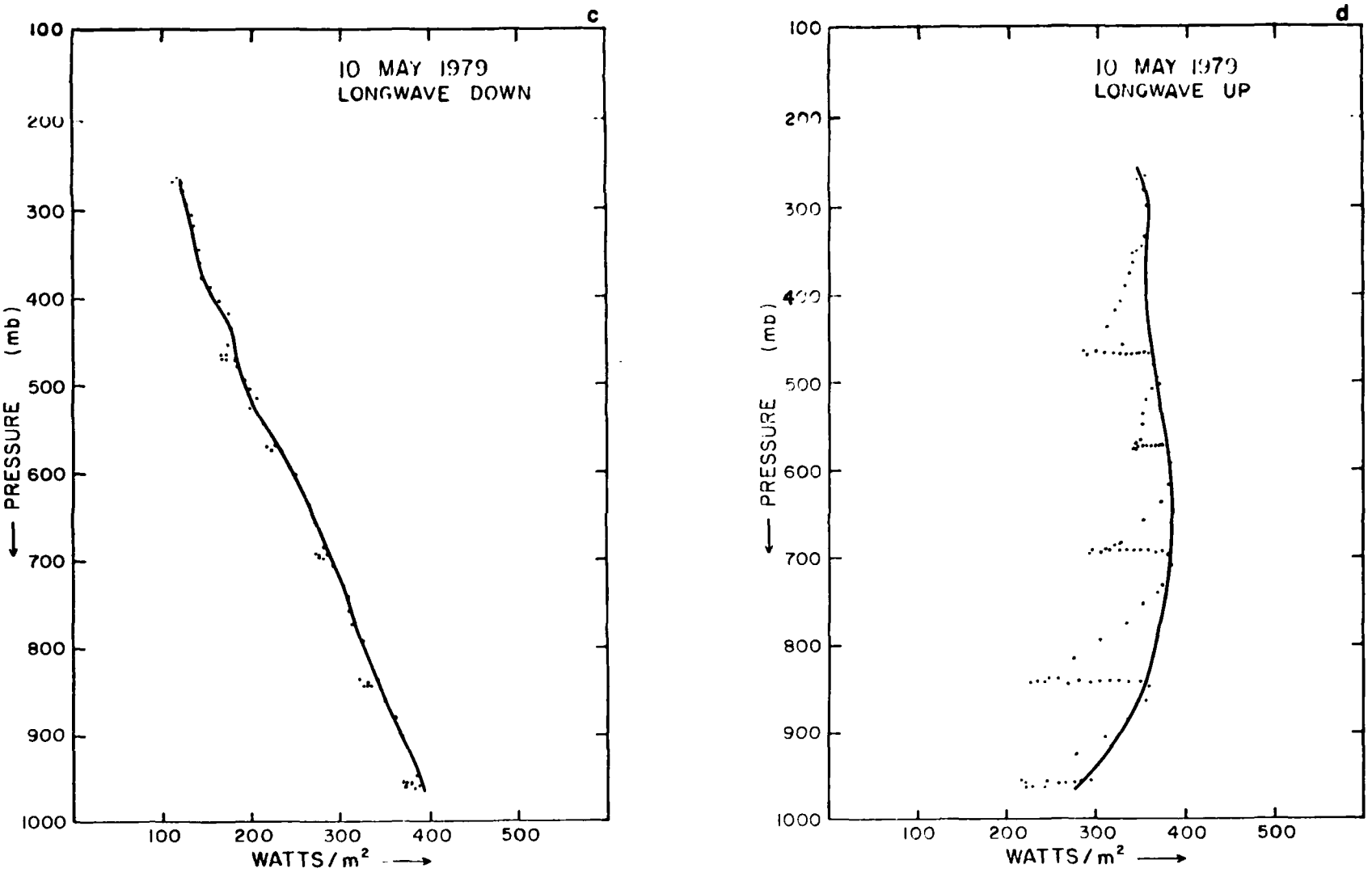

Figure 11 (c,d). Upward and downward longwave irradiance measurements on 10 May plotted as a function of pressure. Units in watts/m^2.

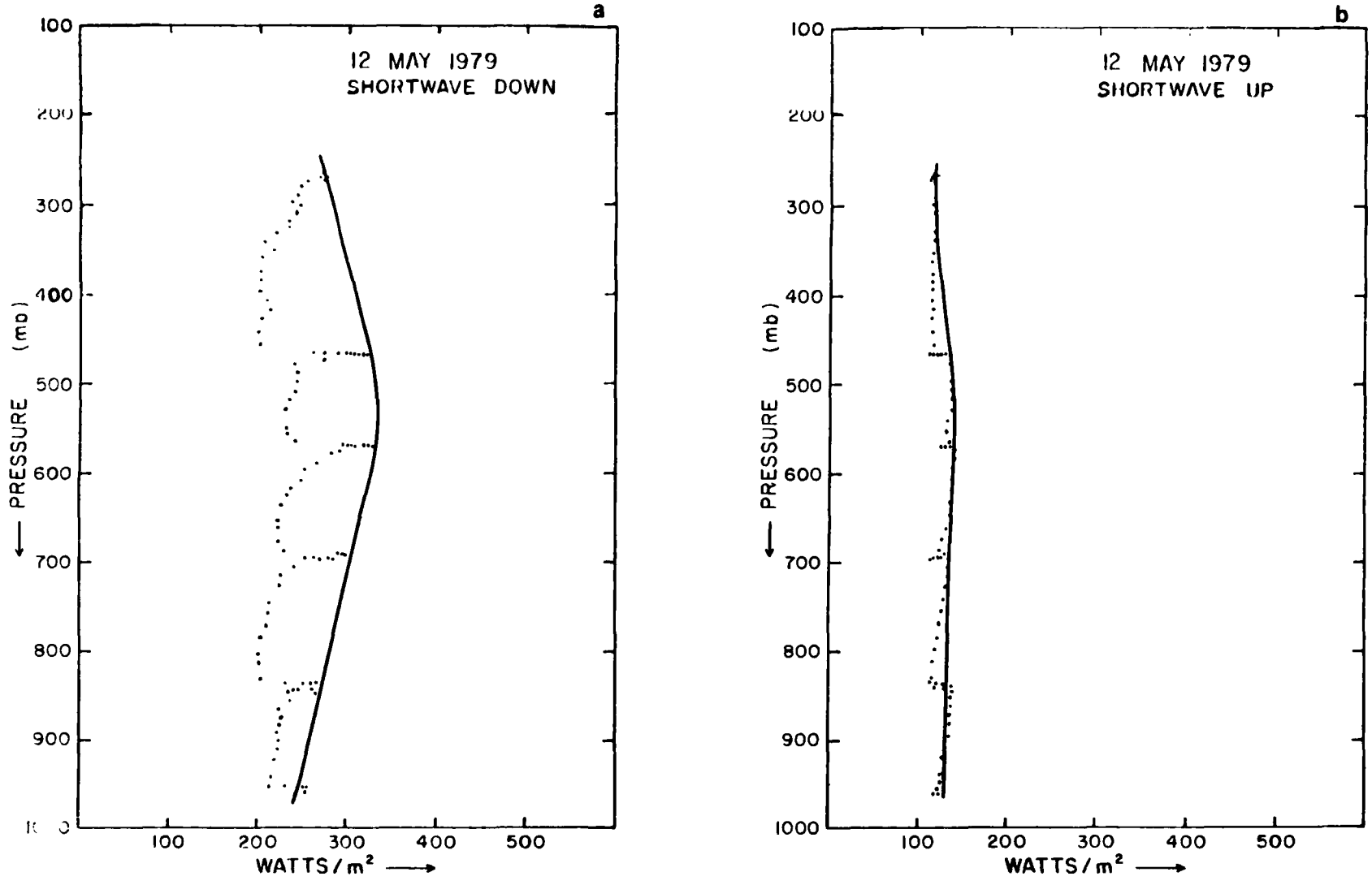

Figure 12 (a,b). Upward and downward shortwave irradiance measurements on 12 May plotted as a function of pressure. Units in watts/m2.

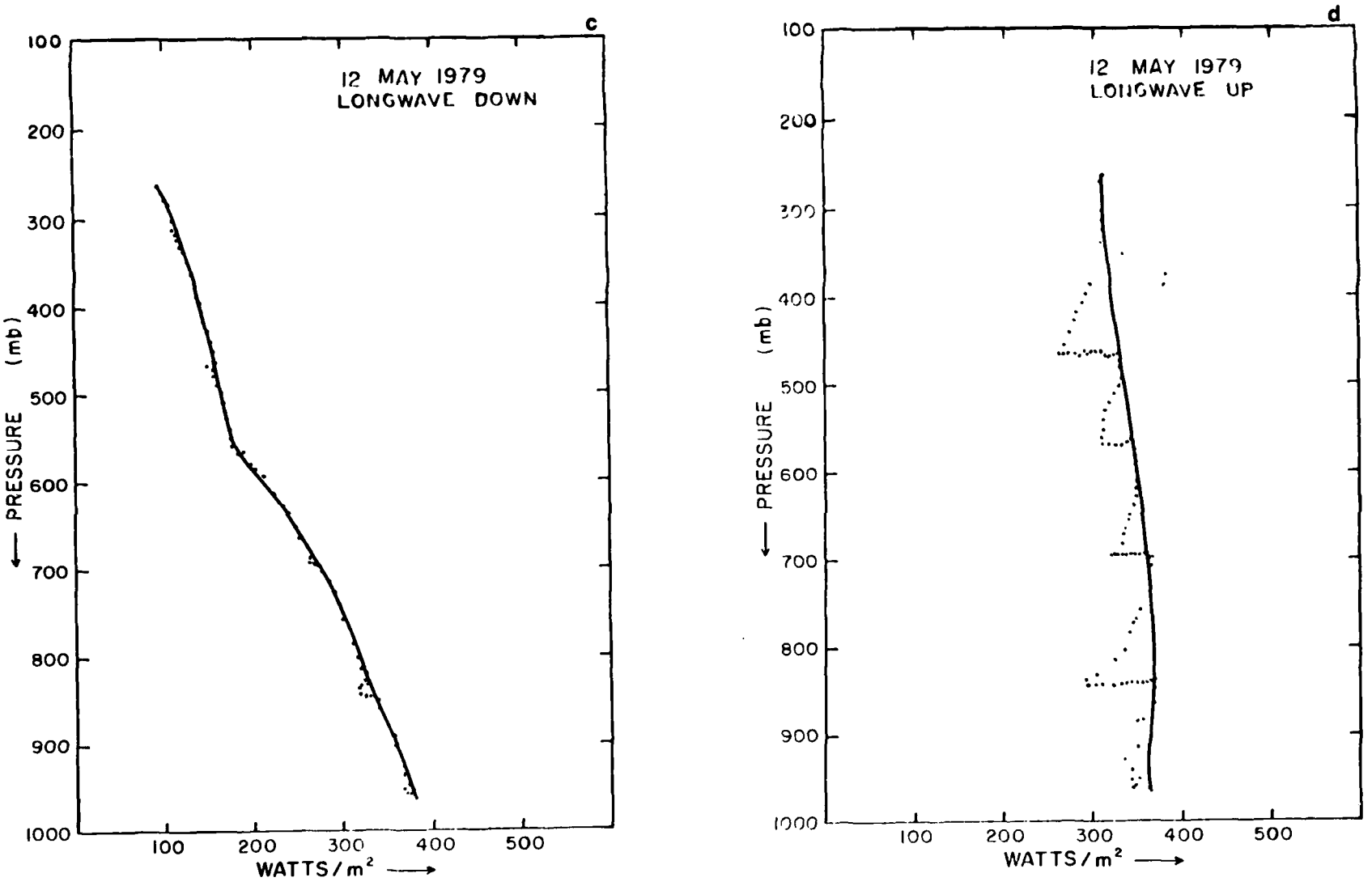

Figure 12 (c,d). Upward and downward longwave irradiance measurements on 12 May plotted as a function of pressure. Units in watts/m^2.

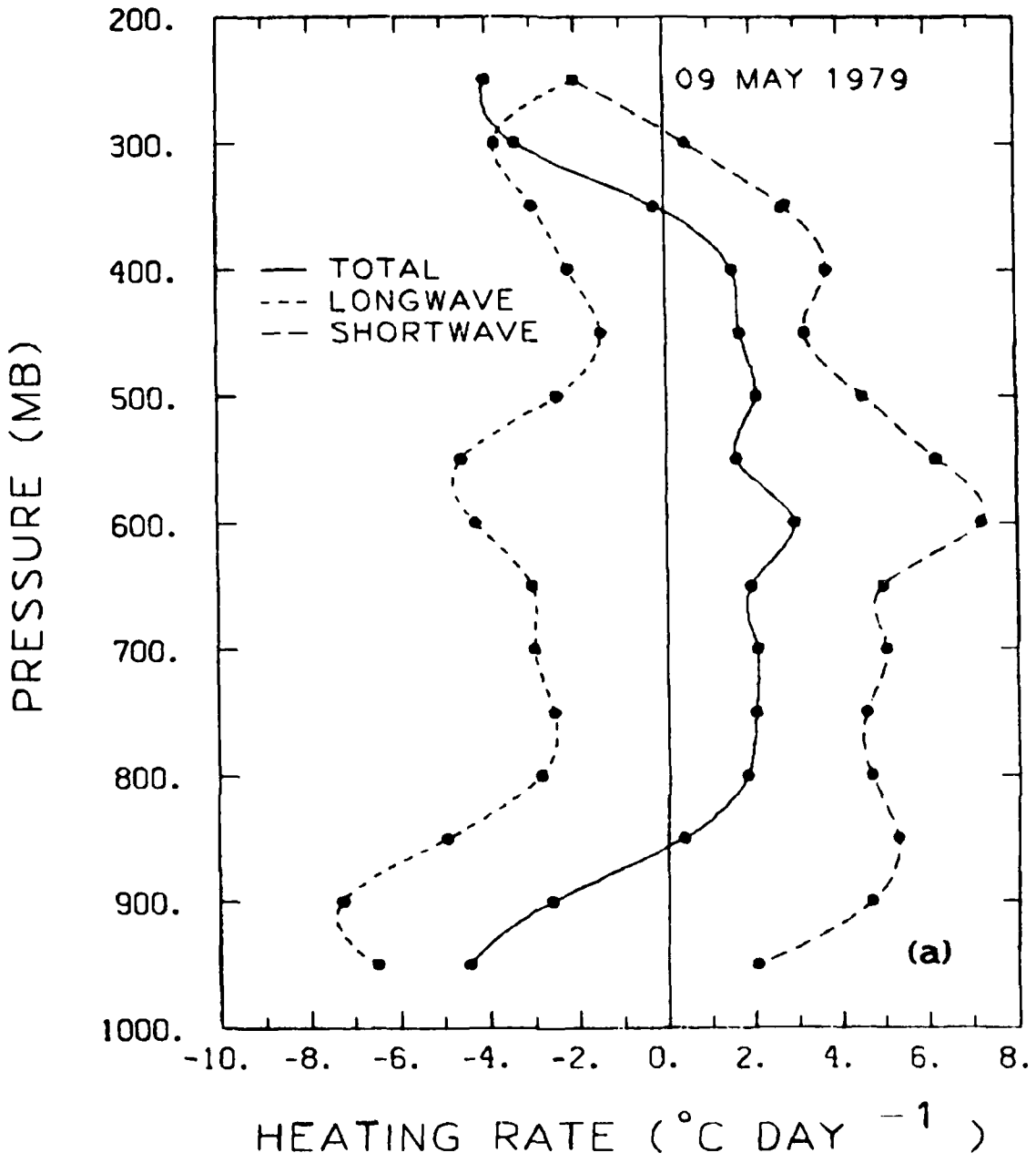

Figure 13 (a). Vertical distribution of the total heating (cooling) rates of the short and longwave radiations on 9 May 1979

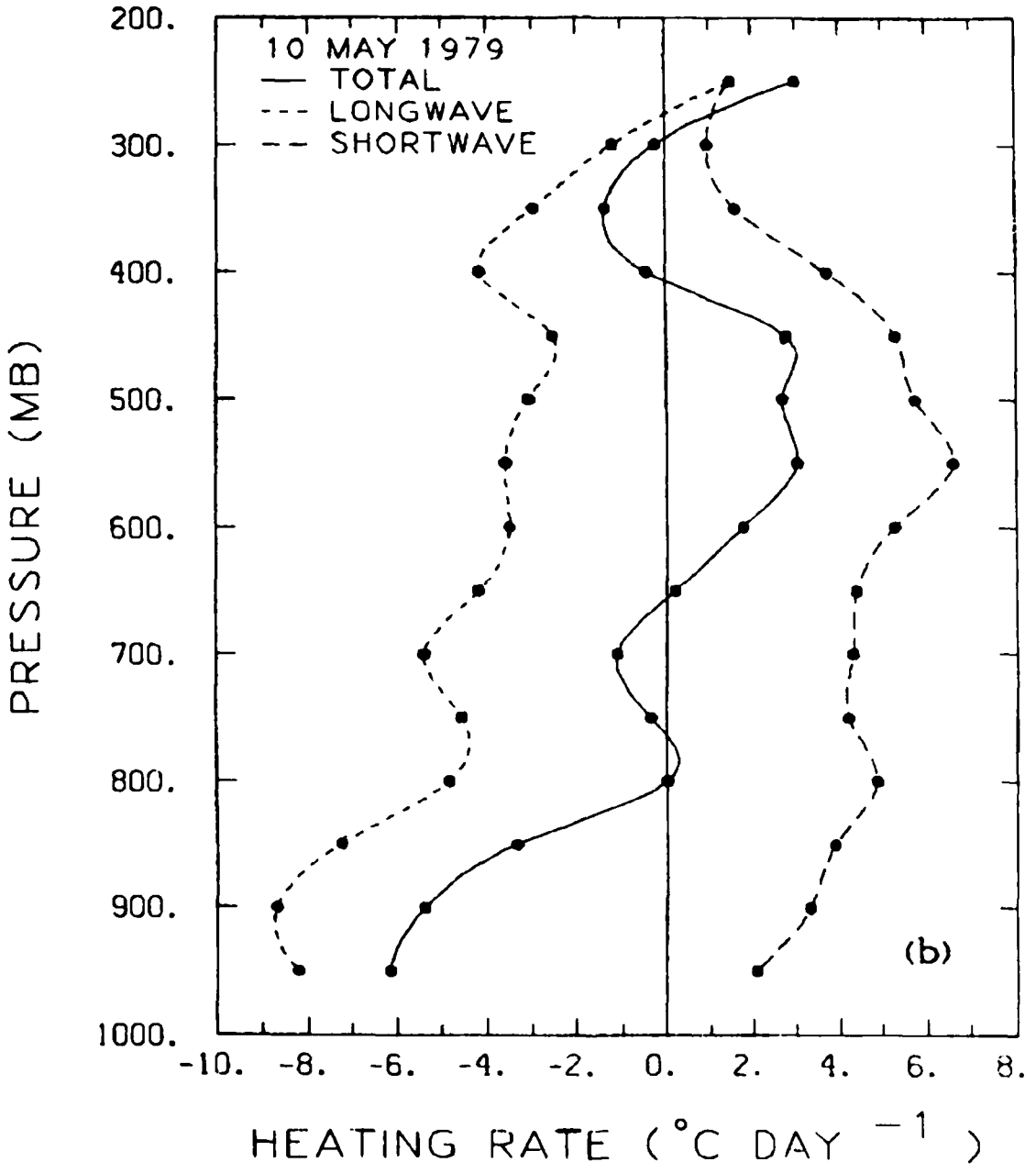

Figure 13 (b). Vertical distribution of the total heating (cooling) rates of the short and longwave radiations on 10 May 1979

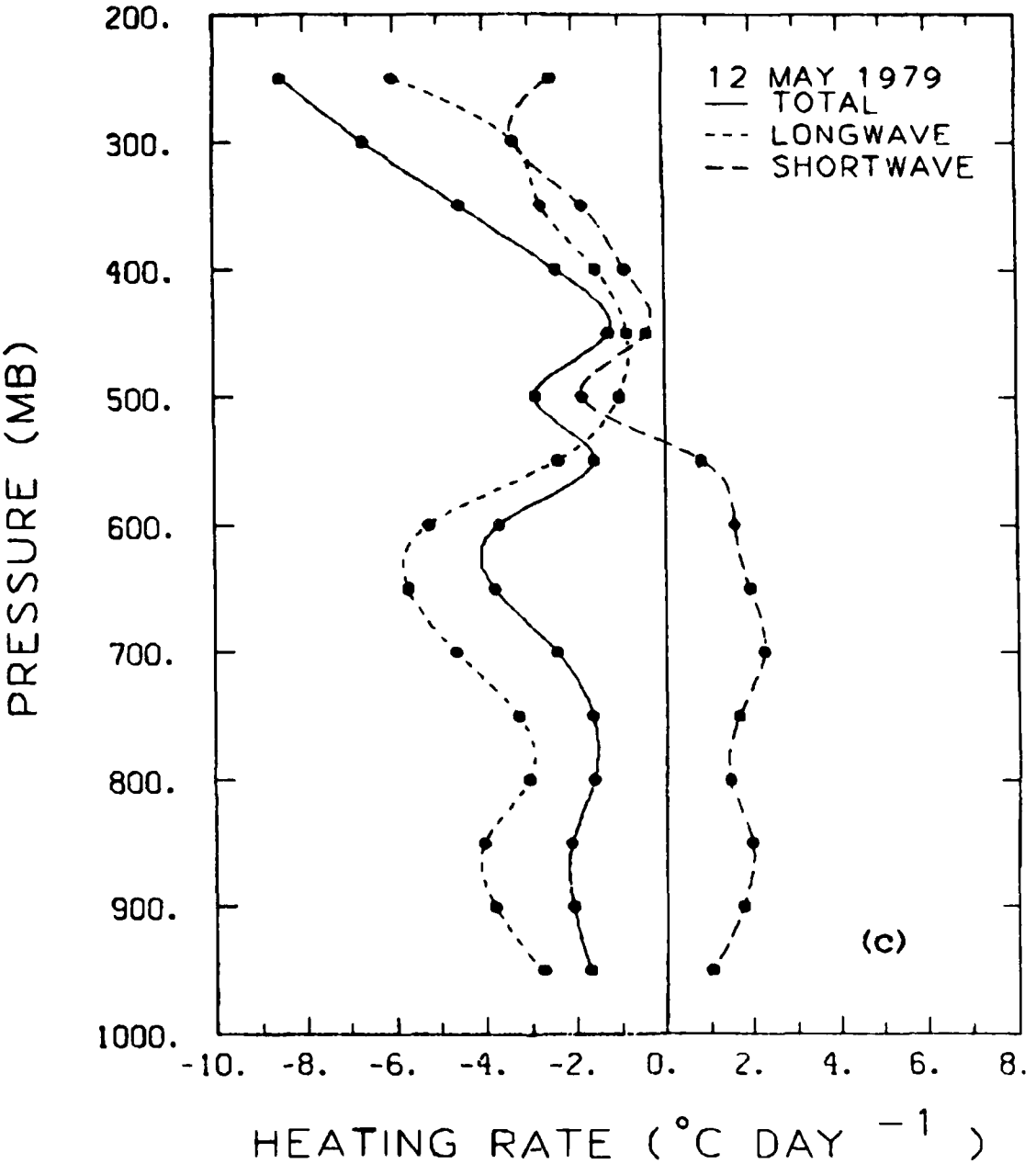

Figure 13 (c). Vertical distribution of the total heating (cooling) rates of the short and longwave radiations on 12 May 1979.

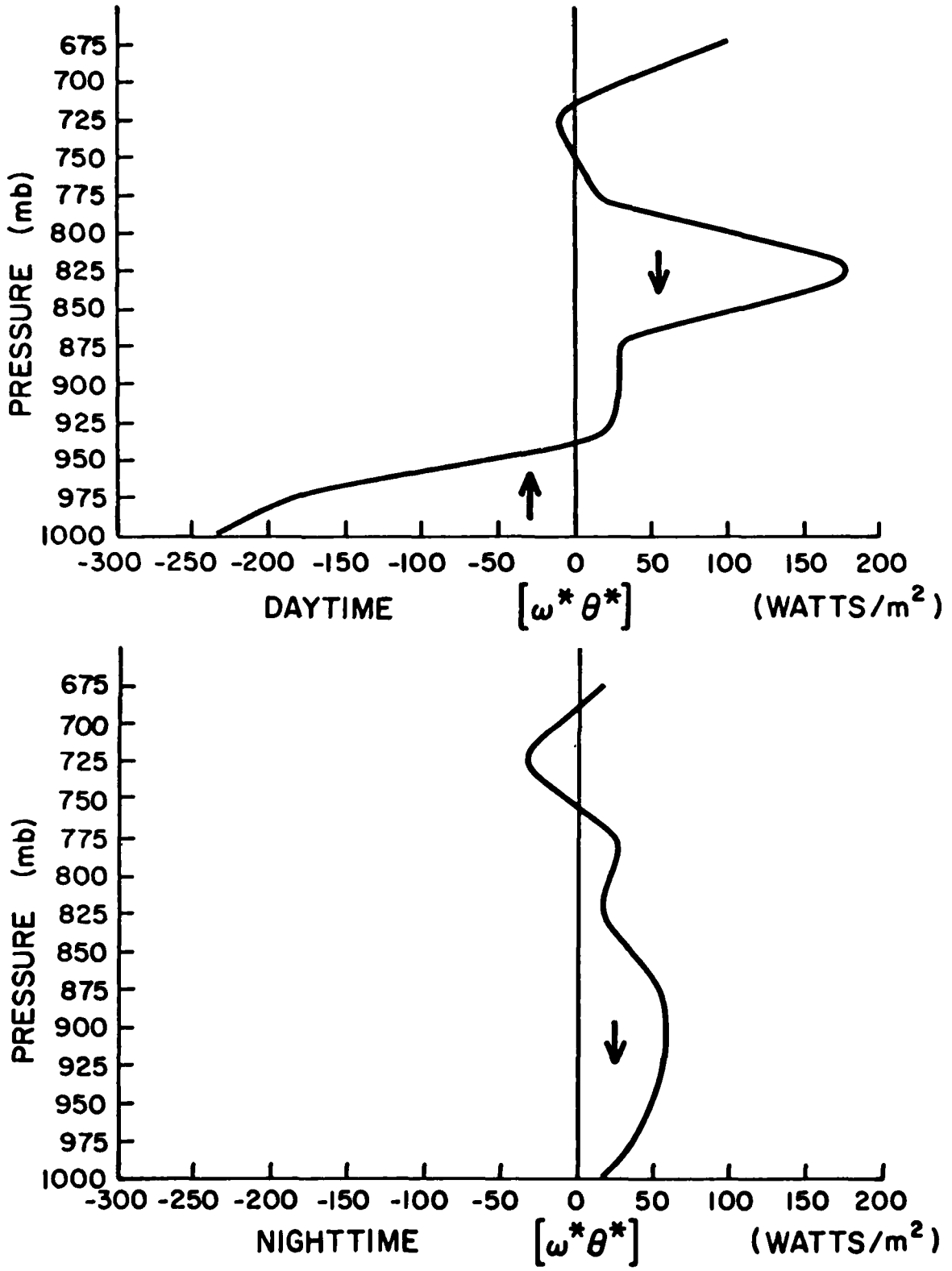

Figure 14. Eddy heat flux for the day and nighttime observations, plotted as a function of pressure. Units are watts/m^2.

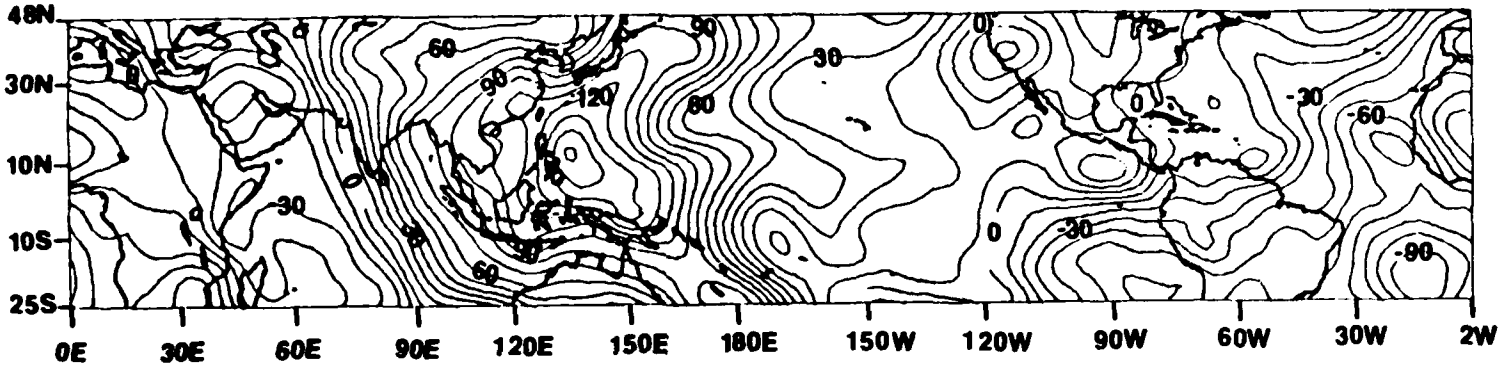

Figure 15. Observed mean of the divergent wind over the global tropical belt for the experimental period averaged over 9, 10, 11, and 12 May 1979 at the 200 mb surface. Units are 10^6 m^2 s^{-1}.

UNCLASSIFIED
SECURITY CLASSIFICATION OF THIS PAGE *(When Data Entered)*

REPORT DOCUMENTATION PAGE		READ INSTRUCTIONS BEFORE COMPLETING FORM
1. REPORT NUMBER NORDA Technical Note 170	2. GOVT ACCESSION NO. A122569	3. RECIPIENT'S CATALOG NUMBER
4. TITLE *(and Subtitle)* The Structure and Energy Budget of the Heat Low Over the Empty Quarter in Saudi Arabia During May 1979		5. TYPE OF REPORT & PERIOD COVERED Final 6. PERFORMING ORG. REPORT NUMBER
7. AUTHOR(s) D. W. Blake S. V. Low-Nam T. N. Krishnamurti J. S. Fein		8. CONTRACT OR GRANT NUMBER(s)
9. PERFORMING ORGANIZATION NAME AND ADDRESS Naval Ocean Research and Development Activity NSTL Station, Mississippi 39529		10. PROGRAM ELEMENT, PROJECT, TASK AREA & WORK UNIT NUMBERS
11. CONTROLLING OFFICE NAME AND ADDRESS Naval Ocean Research and Development Activity NSTL Station, Mississippi 39529		12. REPORT DATE September 1982 13. NUMBER OF PAGES 43
14. MONITORING AGENCY NAME & ADDRESS*(if different from Controlling Office)*		15. SECURITY CLASS. *(of this report)* UNCLASSIFIED 15a. DECLASSIFICATION/DOWNGRADING SCHEDULE
16. DISTRIBUTION STATEMENT *(of this Report)* Distribution Unlimited DISTRIBUTION STATEMENT A Approved for public release; Distribution Unlimited		
17. DISTRIBUTION STATEMENT *(of the abstract entered in Block 20, if different from Report)*		
18. SUPPLEMENTARY NOTES		
19. KEY WORDS *(Continue on reverse side if necessary and identify by block number)* desert MONEX heat budget		
20. ABSTRACT *(Continue on reverse side if necessary and identify by block number)* In this paper we present an analysis of a unique data set over the desert area of Saudi Arabia during the northern summer months. The data set comes from the GARP Monsoon Experiment. The analysis reveals a unique vertical structure of the atmosphere above the heat low. The analysis of the thermodynamic data reveals that a well-mixed layer extends to 650 mb during the daytime and a stable configuration exists during the nighttime. Calculations of divergence and vertical motions show that over this region the entire troposphere is dynamically active		

DD FORM 1 JAN 73 1473 EDITION OF 1 NOV 65 IS OBSOLETE
S/N 0102-LF-014-6601

UNCLASSIFIED
SECURITY CLASSIFICATION OF THIS PAGE *(When Data Entered)*

with strong descending motions above a surface layer about 1 km deep within which rising motions are found in the daytime. Descending motions extend to the surface at night. A description of the vertical distribution of the short and longwave radiative processes over this region, based on detailed aircraft observations, is included. The new results here are the large magnitudes of heating by solar radiation (≈6°C/day) and a comparable cooling by the longwave radiation. The net radiation profile in the daytime exhibits a net warming in the middle troposphere and a net cooling near the surface layer. This contributes to the stabilization of the mixed layer.

This paper addresses the thermodynamic budget over the heat low. Here we examine the role of the horizontal and vertical advective processes, radiative processes and the vertical eddy flux convergence in the maintenance of the tropical stratification.

Satellite observations show that the desert area experiences a net loss of radiation to the outer space, while the thermal stratification remains nearly invariant from one day to the next. This study shows that a crucial element in the maintenance of the stratification is the import of heat into this region in the tropical upper troposphere. This energy supply most likely comes from planetary scale divergent circulations.

END

FILMED

1-83

DTIC